

See discussions, stats, and author profiles for this publication at: <https://www.researchgate.net/publication/51577604>

# Kinetic Modeling of Ethane Pyrolysis at High Conversion

ARTICLE *in* THE JOURNAL OF PHYSICAL CHEMISTRY A · AUGUST 2011

Impact Factor: 2.69 · DOI: 10.1021/jp206503d · Source: PubMed

---

CITATIONS

8

READS

89

## 5 AUTHORS, INCLUDING:



[Chenguang Wang](#)  
Chinese Academy of Sciences

19 PUBLICATIONS 202 CITATIONS

[SEE PROFILE](#)



[Anthony M Dean](#)  
Colorado School of Mines

158 PUBLICATIONS 3,933 CITATIONS

[SEE PROFILE](#)

# Kinetic Modeling of Ethane Pyrolysis at High Conversion

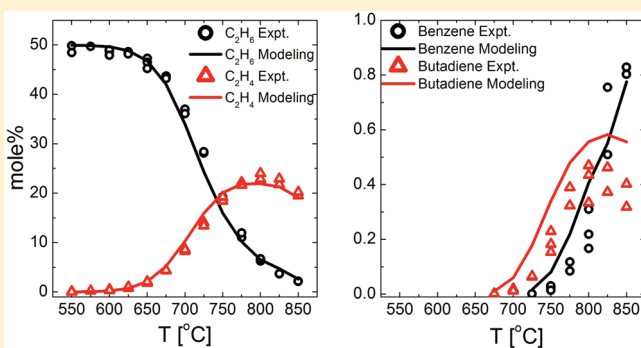
Chen Xu,<sup>†</sup> Ahmed Sultan Al Shoaibi,<sup>‡</sup> Chenguang Wang,<sup>†</sup> Hans-Heinrich Carstensen,<sup>†</sup> and Anthony M. Dean<sup>\*,†</sup>

<sup>†</sup>Department of Chemical Engineering, Colorado School of Mines, Golden, Colorado 80401, United States

<sup>‡</sup>Chemical Engineering Department, Petroleum Institute, Abu Dhabi, United Arab Emirates

 Supporting Information

**ABSTRACT:** The primary objective of this study is to develop an improved first-principle-based mechanism that describes the molecular weight growth kinetics observed during ethane pyrolysis. A proper characterization of the kinetics of ethane pyrolysis is a prerequisite for any analysis of hydrocarbon pyrolysis and oxidation. Flow reactor experiments were performed with ~50/50 ethane/nitrogen mixtures with temperatures ranging from 550 to 850 °C at an absolute pressure of ~0.8 atm and a residence time of ~5 s. These conditions result in ethane conversions ranging from virtually no reaction to ~90%. Comparisons of predictions using our original mechanism to these data yielded very satisfactory results in terms of the temperature dependence of ethane conversion and prediction of the major products ethylene and hydrogen. However, there were discrepancies in some of the minor species concentrations that are involved in the molecular weight growth kinetics. We performed a series of CBS-QB3 analyses for the C<sub>3</sub>H<sub>7</sub>, C<sub>4</sub>H<sub>9</sub>, and C<sub>6</sub>H<sub>9</sub> potential energy surfaces to better characterize the radical addition reactions that lead to molecular weight growth. We also extended a published C<sub>6</sub>H<sub>9</sub> PES to include addition of vinyl to butadiene. The results were then used to calculate pressure-dependent rate constants for the multiple reaction pathways of these addition reactions. Inclusion of the unadjusted rate constants resulting from these analyses in the mechanism significantly improved the description of several of the species involved in molecular weight growth kinetics. We compare the predictions of this improved model to those obtained with a consensus model recently published as well as to ethane steam cracking data. We find that a particularly important reaction is that of vinyl addition to butadiene. Another important observation is that several radical addition reactions are partially equilibrated. Not only does this mean that reliable thermodynamic parameters are essential for an accurate model, but also that the reaction set describing molecular weight growth chemistry must include a final product that is sufficiently stable to shift the equilibrium toward this product despite the decrease in entropy that accompanies molecular weight growth. Another reaction, H addition to olefins, was found to inhibit molecular weight growth by leading to the production of a lower olefin plus methyl radicals.



## 1. INTRODUCTION

A proper characterization of the kinetics of ethane pyrolysis is a prerequisite for any analysis of hydrocarbon pyrolysis and oxidation. The presence of the C–C bond makes ethane the simplest model compound for higher alkanes. As the second most abundant component in natural gas, its chemistry is essential to describe natural gas ignition and combustion. Ethane pyrolysis in the presence of steam is widely practiced commercially to produce ethylene and higher olefins. Despite its importance, surprisingly little is known about ethane pyrolysis kinetics under high conversion conditions. In particular, there remains substantial uncertainty regarding the details of the molecular weight growth reactions that can ultimately lead to formation of carbonaceous deposits.

Conversely, ethane pyrolysis has been extensively studied at low conversion. Indeed, ethane dissociation and the reverse methyl recombination reactions are frequently used as reference

reactions in kinetic studies of unimolecular reactions.<sup>1–4</sup> Thermal decomposition experiments have been performed in shock tubes at high temperatures by Oehlschlaeger et al.,<sup>5</sup> Kiefer et al.,<sup>6</sup> Hidaka et al.,<sup>7</sup> and Tranter et al.<sup>8</sup> These studies focused mostly on the primary reaction steps.

Sabbe et al.<sup>9</sup> developed an ethane steam cracking model based on a first principle-based group additivity method and compared the predictions to pilot and industrial scale steam cracking reactors. The coil outlet temperature varied from ~790 to 890 °C, and the coil outlet pressure was ~2 atm. Their unadjusted model correctly accounts for ethane conversion and many of the products. However, the predicted yields for methane and propene are significantly underestimated. The

**Received:** July 9, 2011

**Revised:** August 16, 2011

**Published:** August 17, 2011

authors suggest that perhaps one reason for the underpredictions is that only high-pressure rate constants were used in the kinetic models and the effect of pressure dependency was not considered.

Glasier and Pacey<sup>10</sup> performed ethane pyrolysis experiments at ~910 °C at high levels of conversion and measured gaseous product formation as well as the rate of pyrolytic carbon formation. Matheu and Grenda<sup>11</sup> developed a kinetic model that captured many of the observed kinetic features of these high conversion data. However, this model overpredicted the butadiene mole fraction by approximately a factor of 2 while underpredicting the benzene mole fraction by approximately a factor of 3. In a subsequent publication,<sup>12</sup> they discussed potential improvements to the model in terms of radical disproportionation reactions and suggested the need for additional research to better characterize the molecular weight growth kinetics.

One area where such molecular growth reactions of ethane are important is in the anode channel of a solid-oxide fuel cell (SOFC) that is operating on natural gas. Typical operating temperatures for SOFCs range from 600 to 800 °C. At these temperatures, thermal decomposition of ethane (or higher hydrocarbons) within the anode channel could be significant and thus influence SOFC operation. One such effect could be that the olefins produced will react differently than alkanes with the catalyst (typically nickel) within the anode. Another possibility that raises substantial concerns is the potential for formation of carbonaceous deposits. Such deposits may be formed via gas-phase reactions as well as catalytic surface chemistry mechanisms. In the gas phase, molecular weight growth reactions may lead to PAH formation as observed in the Glasier and Pacey<sup>10</sup> experiments. These might then condense on the catalyst within the anode where they might inhibit catalytic activity and/or restrict transport of the gases to the electrochemically active region. Characterization of such reactions can provide guidance as to the combinations of temperature, residence time, and fuel composition required to avoid this mode of deposit formation in SOFC operation. Alternatively, this knowledge might suggest approaches to mitigate such deposit formation by identifying a way to interrupt the molecular weight growth reaction sequence. Similar considerations apply to the ethane steam cracking process, where deposit formation on the tube walls requires occasional decoking procedures to avoid excessive tube wall temperatures.

There is an important difference between the species involved in molecular weight growth near 800 °C versus those responsible for soot formation during fuel-rich combustion. The lower temperature results in a much lower concentration of acetylene, the species that plays a key role in soot production at higher temperatures. This difference implies that ethylene might be the dominant species involved in the radical addition reactions that lead to molecular weight growth at the lower temperature.<sup>13</sup> In this context, ethane pyrolysis offers a good opportunity to begin to analyze molecular weight growth in alkanes at lower temperatures because the dominant product of ethane pyrolysis is ethylene. At the same time, the number of reactions and species to consider in the mechanism will be smaller than required for an analysis of the pyrolysis of higher alkanes.

The primary objective of the present study is to develop an improved first-principles-based mechanism that describes the molecular weight growth kinetics observed during ethane pyrolysis. We first present experimental results obtained with ~50/50

ethane/nitrogen mixtures with temperatures ranging from 550 to 850 °C at an absolute pressure of ~0.8 atm and a residence time of ~5 s. These conditions result in ethane conversions ranging from virtually no reaction to ~90% consumption. The measured mole fractions exhibit consistently good carbon and hydrogen mass balances. Species up to naphthalene and acenaphthalene were observed in small yields at the highest levels of conversion. Comparison to predictions of these data using our original mechanism yielded very satisfactory results in terms of the temperature dependence of ethane conversion and the prediction of the major products ethylene and hydrogen. However, there were some discrepancies in the comparison of some of the minor species that are involved in the molecular weight growth kinetics. Sensitivity and rate analyses were used to identify the important reactions. Many of these are hydrogen abstraction reactions with rate constants that are consistent with both experimental and theoretical analyses. Another group of sensitive reactions is pressure-dependent radical addition reactions where the available literature data are quite sparse. Thus, we initiated a series of CBS-QB3 analyses for the C<sub>3</sub>H<sub>7</sub>, C<sub>4</sub>H<sub>7</sub>, and C<sub>4</sub>H<sub>9</sub> potential energy surfaces. We also extended the C<sub>6</sub>H<sub>9</sub> PES results of Sharma et al.<sup>14</sup> to include the addition reaction of vinyl to butadiene. The results were then used to calculate pressure-dependent rate constants for the multiple reaction pathways of these addition reactions. Inclusion of the unadjusted rate constants resulting from these analyses in the mechanism significantly improved the description of several of the "problem" species. We also compare the predictions of this improved model to those obtained with a consensus model recently published.<sup>15</sup> Although the focus of that model development was combustion, it necessarily contains a pyrolysis subset. We then use our updated model to simulate the ethane steam cracking data of Sabbe et al.<sup>9</sup> Finally, we discuss the important features that lead to the improved description of molecular weight growth kinetics and point out areas where additional research is warranted.

## 2. EXPERIMENTAL METHODS

Ethane pyrolysis was studied in a tubular quartz flow reactor at ambient pressure (~0.8 atm) over a temperature range 550–850 °C. Quartz was used to minimize the impact of surface-catalyzed reactions. The reactor is 34 cm long with an inner diameter of 6 mm. The flow reactor was housed in a cylindrical oven equipped with three independently PID controlled electrical resistance heaters (Eurotherm model 2116e). To prevent condensation of high molecular weight products, additional resistive heating was supplied to the tubing from the reactor exit region to the sampling valves of the online GCs. Temperatures along the reactor centerline were measured under a nitrogen flow with a K-type (Cr/Ni) thermocouple (OMEGA KMQXL-062G-24) that was moved axially along the reactor length at 1 cm intervals. The thermocouple bead was coated with high temperature alumina adhesive to inhibit catalytic reactions on the thermocouple surface. The work of Villano et al.<sup>16</sup> demonstrated that temperature profiles measured under nitrogen flow and reactive flow are almost identical. As shown in Figure 1, the temperature was very constant in the middle zone of the reactor. For all of the runs, the maximum deviation of the temperature from the average was less than 2 K in the constant temperature region of the reactor. The thermocouple was removed in the ethane pyrolysis experiments.

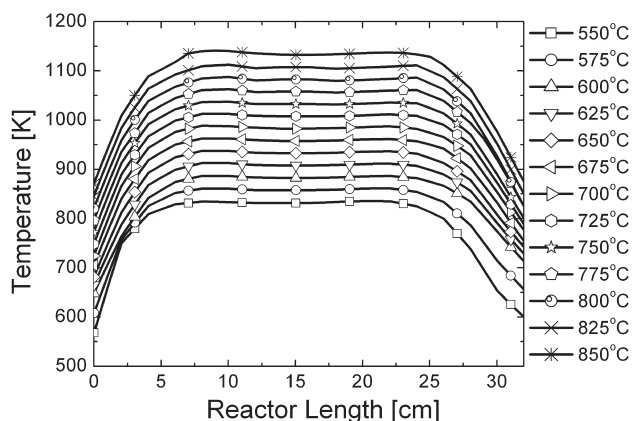


**Figure 1.** Experimental temperature profiles measured along the centerline of the tubular reactor.

Ethane was diluted in nitrogen, and the initial  $\text{C}_2\text{H}_6/\text{N}_2$  mole ratio was set at  $\sim 50/50$ . Nitrogen (General Air, 99.998%) and ethane (Matheson TriGas, 99.95%) were supplied from compressed gas cylinders. The reactants were metered into the reactor by means of mass flow controllers (Alicat Scientific MC Series 16) calibrated with a bubble flow meter. The uncertainty in the gas flows regulated by the mass flow controllers was measured to be within  $\pm 1\%$ . The reactant gas flows were mixed in a 150 mL cylinder before introduction into the reactor. Nominal residence times of the reacting mixture in the hot zone were calculated using the 1-D plug flow assumption by scaling the gas velocity to the variation in gas density due to temperature and mole changes along the reactor. The total reactant flow rate was maintained at 30 SCCM, which corresponds to a nominal residence time of  $\sim 5$  s in the hot zone (assuming an increase of  $\sim 40\%$  in the total number of moles).

Three different sets of ethane pyrolysis experiments were performed. In the first series, the reactor effluent was analyzed with a GC (HP 5890 Series II), and the products were quantified using a thermal conductivity detector (TCD) and a flame ionization detector (FID). Three columns (HayeSep R, Carboxen 1000 and Supelco SPB-1) were used to separate nitrogen, hydrogen, light, and heavy hydrocarbons. Details have been described previously in Randolph et al.<sup>17</sup> and Al Shoaibi.<sup>18</sup> For several experiments, the reactor effluent was directed to a MKS Cirrus LM 99 mass spectrometer where the observed cracking pattern was used to help identify the higher molecular weight species.

In the second and third sets of experiments, the reactor effluent was analyzed with both the HP 5890 Series II GC and a GC-MS/FID (Trace GC). Nitrogen, hydrogen, and light hydrocarbons were identified with the 5890 GC using a tandem 4.6 m  $\times$  2.1 m i.d. stainless steel packed Carboxen 1000 column followed by a Supelco 4.6 m  $\times$  2.1 m i.d. stainless steel packed Porapak R column with argon carrier gas. The heavier hydrocarbons were diverted from the Carboxen column and vented. For the second set of experiments, the time at which the value was switched to divert higher hydrocarbons was set so that hydrogen, nitrogen, and methane were measured. The delay time was increased in the third set of experiments to allow detection of the  $\text{C}_2$  species (including acetylene). Heavier hydrocarbons were analyzed on the Trace GC using a 60 m J&W Fisher DB-1 0.25 mm i.d. fused silica capillary column (2.5  $\mu\text{m}$  film) with helium as

the carrier gas and nitrogen as the makeup gas. (On this column, the much larger ethylene peak obscured the small acetylene peak.) For the 5890 GC, the oven temperature program was set at 40 °C for 5 min followed by an increase of 20 °C/min up to 220 °C and remained fixed at 220 °C for 20 min. The Trace GC program starts at 40 °C for 5 min, increases to 200 at 20 °C/min, and remains fixed at this temperature for 35 min. The two GCs provide dual detection of methane and some  $\text{C}_2$  species; the typical agreement in the measured mole fractions was within  $\sim 2\%$  (relative). The mass spectrometer on the Trace instrument was used to aid identification of the higher molecular weight species.

The response factors were calibrated frequently using prepared standard gas mixtures. The GC peak measurement error was observed to be less than  $\pm 1\%$  for hydrogen and nitrogen with the TCD detector and less than  $\pm 1.5\%$  for  $\text{C}_1-\text{C}_4$  aliphatic species with the FID detectors. Calibration of 1,3-butadiene was complicated by fluctuations in the MFC flow rate. This leads to a larger measurement error ( $\sim 5\%$  relative error) for this species. The reported mole fractions of methane were taken from the Trace GC because it has better separation. We found it very difficult to obtain accurate mole fraction measurements for acetylene on the HP 5890. The acetylene signal was not constant during repeated calibration runs; similarly the observed deviations of the acetylene signal during pyrolysis experiments were generally significantly higher than the run-to-run fluctuations observed for any other species. The reasons for these erratic measurements are still under investigation. As a result, our reported acetylene mole fractions should be considered as semiquantitative. The calibration of the liquid  $\text{C}_5-\text{C}_8$  species was performed by dissolving the species in toluene, with the solution then pumped into a stainless steel vessel by an HPLC pump. This vessel was wrapped with a PID controlled electrical resistance heater (Eurotherm model 2116e), and the temperature was monitored at 160 °C. Cyclopentadiene was calibrated by employing dicyclopentadiene (DCPD, Sigma-Aldrich) as the precursor; it undergoes a retro-Diels–Alder reaction to yield cyclopentadiene above 150 °C. Other calibrated unsaturated species included cyclopentene, benzene, 1,3-cyclohexadiene, toluene, and styrene, all purchased from Sigma-Aldrich. The accuracy of liquid fuel calibration data was estimated to be  $\sim 5\%$  (relative).

### 3. ORIGINAL MODEL DESCRIPTION

The reaction mechanism used for the initial predictions consisted of 224 species and 1722 reactions. This mechanism does not include any oxygenated species. It is an updated version of that described by Randolph and Dean<sup>17</sup> in their analysis of *n*-hexane pyrolysis. The major update involved the use of rate rules based on the results of CBS-QB3 calculations<sup>19</sup> to assign the rate constants for some of the hydrogen abstraction reactions. The elementary reactions involved in the model can be generally classified into five categories: (1) initial dissociation reactions leading to the formation of free radicals and the reverse recombination reactions, (2) hydrogen abstraction reactions, (3) Addition reactions between a free radical and an unsaturated species to generate a new free radical and the reverse  $\beta$ -scission reactions, (4) disproportionation reactions, and (5) other reactions such as Diels–Alder and retro-Diels–Alder reactions. Reactions in categories (1), (3), and (5) are pressure-dependent, and multiple reaction channels are possible. For these pressure-dependent

**Table 1.** Experimental Data Obtained from Ethane Pyrolysis<sup>a</sup>

species	average experimentally observed mole %								
	600 °C	625 °C	650 °C	675 °C	700 °C	725 °C	750 °C	775 °C	800 °C
H <sub>2</sub>	0.37	0.82	2.00	4.44	8.96	14.5	20.2	24.6	27.5
N <sub>2</sub>	50.6	50.4	49.6	48.2	46.1	43.2	40.5	38.4	36.9
CH <sub>4</sub> TCD	0	0	0	0	0.22	0.77	1.73	3.42	5.67
CH <sub>4</sub> FID	0	0.01	0.03	0.08	0.25	0.68	1.60	3.30	5.44
C <sub>2</sub> H <sub>6</sub>	48.7	48.7	47.3	43.7	37.0	28.2	19.0	11.0	6.26
C <sub>2</sub> H <sub>4</sub>	0.38	0.77	1.81	4.30	8.66	14.1	19.1	22.2	22.6
C <sub>3</sub> H <sub>6</sub>	0	0	0	0.044	0.052	0.093	0.233	0.323	0.342
C <sub>3</sub> H <sub>8</sub>	0	0	0	0	0.0188	0.0178	0.0356	0.0386	0.0000
allene	0	0	0	0	0	0	0	0	0.0225
1,3-C <sub>4</sub> H <sub>6</sub>	0	0	0	0	0.0197	0.0623	0.230	0.390	0.4707
2-C <sub>4</sub> H <sub>8</sub>	0	0	0	0	0	0	0	0	0.0173
n-C <sub>4</sub> H <sub>10</sub>	0	0	0.0089	0.0223	0.0451	0.0461	0.0570	0.0426	0.0182
cyclopentadiene	0	0	0	0	0	0	0.0377	0.0954	0.137
benzene	0	0	0	0	0	0	0.0248	0.118	0.310
cyclohexadiene	0	0	0	0	0	0	0	0	0.0062
toluene	0	0	0	0	0	0	0	0.0186	0.0310
styrene	0	0	0	0	0	0	0	0.0062	0.0248
indene	0	0	0	0	0	0	0	0	0.0124
naphthalene	0	0	0	0	0	0	0	0	0.0248
total	100.1	100.7	100.7	100.8	101.1	100.9	101.0	100.5	100.1
C <sub>out</sub> /C <sub>in</sub>	0.99	1.00	1.01	1.02	1.02	1.02	1.01	0.98	0.97
H <sub>out</sub> /H <sub>in</sub>	0.99	1.00	1.01	1.02	1.02	1.02	1.01	0.99	0.99

<sup>a</sup> Set 1: C<sub>2</sub>H<sub>6</sub>/N<sub>2</sub> = 49.6/50.7.

chemically activated reactions, rate constants for the various reaction pathways were fitted to Chebyshev polynomials because these provide a better description for multichannel multiwell reaction systems.<sup>20</sup> These pressure-dependent rate constants were calculated using a Quantum Rice Ramsperger Kassel analysis to calculate  $k(E)$  coupled with the modified strong collision approximation to account for collisional deactivation (QRRK/MSC).<sup>21</sup> Additional details of this approach have been published previously.<sup>22</sup> The rate constants for the reverse reactions were calculated on the basis of forward reaction rate constants, using the temperature-dependent equilibrium constant computed from the thermochemical data. The thermodynamic properties were obtained from literature values when reliable values were available. Otherwise, these data were either estimated on the basis of the group additivity method using THERM<sup>23</sup> or computed using electronic structure theory. The quartz reactor was modeled using the plug flow reactor module in CHEMKIN PRO,<sup>24</sup> assuming no wall effects. The measured temperature-distance profiles were input in the calculations.

#### 4. RESULTS AND DISCUSSION

**4.1. Experimental and Original Modeling Results.** The experimental data are listed in Tables 1–3 and summarized in Figure 2. For each temperature, typically three measurements were made, and the averages are reported. The sums of the measured mole fractions as well as calculated carbon and hydrogen balances are also reported in the tables. In Table 1, one sees that the measured total mole fraction for the set 1 experiments sum to 100% within the expected experimental error over the temperature range 600–800 °C. Because any high molecular

weight species with very long retention times that might not have been detected would only be produced at the high conversions achieved at the higher temperatures, the constant mole fraction sum over the temperature range indicates that the mole fractions of any species that were not observed were on the order of 1% or less. A qualification to this statement is that some species, for example, acetylene, might be hidden under larger peaks, for example, ethylene, but their similar FID response factors would lead to a similar total C<sub>2</sub> sum. The measured carbon and hydrogen balances agree within the experimental error over most of the temperature range and only begin to show a deviation at the highest temperatures, perhaps suggesting a slight loss of product due to deposit formation at the highest conversion levels. This is consistent with the observation that a thin black film was observed on the reactor walls after experiments were run for several hours at 800 °C.

The results of the first set of experiments with the GC/MS system (set 2) are shown in Table 2. These data were collected at the same pressure and residence time as those in Table 1, but a wider temperature range (550–850 °C) was sampled. Again, we see that the sums of the observed mole fractions are very close to 100%, indicating that the mole fractions of species with retention times outside of the detected range were negligible. There is a systematic decline in both carbon and hydrogen mass balances above 750 °C, indicating the likelihood of some deposit formation. However, even the most extreme deviation in the carbon mass balance (0.88 at 850 °C) leads to a mole fraction of deposit of less than 1% (assuming the number of carbon atoms in a species deposited was 12). For the wider temperature range of this data set, we see an even larger range of ethane conversion, with correspondingly larger amounts of high molecular weight

**Table 2.** Experimental Data Obtained from Ethane Pyrolysis<sup>a</sup>

species	average experimentally observed mole %												
	550 °C	575 °C	600 °C	625 °C	650 °C	675 °C	700 °C	725 °C	750 °C	775 °C	800 °C	825 °C	850 °C
H <sub>2</sub>	0.31	0.36	0.71	1.23	2.38	4.76	8.91	14.6	20.2	24.8	28.0	30.1	31.8
N <sub>2</sub>	50.1	50.0	50.1	49.8	48.9	47.6	45.6	43.2	40.4	38.2	36.5	35.5	35.1
CH <sub>4</sub> (trace)	0.27	0.28	0.27	0.28	0.29	0.33	0.46	0.82	1.62	2.96	5.02	7.39	9.76
C <sub>2</sub> H <sub>6</sub>	49.9	49.7	49.0	48.2	46.5	43.2	37.0	28.4	19.3	12.0	6.6	3.7	2.2
C <sub>2</sub> H <sub>4</sub>	0.13	0.26	0.52	1.05	2.14	4.41	8.25	13.4	18.4	21.6	22.9	21.8	19.5
allene	0	0	0	0	0	0	0	0	0.0032	0.0085	0.0164	0.0230	0.0273
propyne	0	0	0	0	0	0	0	0	0.0013	0.0034	0.0064	0.0087	0.0098
C <sub>3</sub> H <sub>6</sub>	0	0	0	0	0.0016	0.0083	0.0329	0.0962	0.194	0.273	0.293	0.245	0.198
C <sub>3</sub> H <sub>8</sub>	0	0	0	0	0	0.0017	0.0036	0.0094	0.0177	0.0227	0.0206	0.0142	0.0086
1,3-C <sub>4</sub> H <sub>6</sub>	0	0	0	0	0	0.0022	0.0157	0.0660	0.183	0.324	0.435	0.462	0.403
1-C <sub>4</sub> H <sub>8</sub>	0	0	0	0	0	0.0034	0.0088	0.0158	0.0220	0.0221	0.0183	0.0125	0.0072
2-C <sub>4</sub> H <sub>8</sub>	0	0	0	0	0	0	0	0.0051	0.0119	0.0176	0.0196	0.0173	0.0126
n-C <sub>4</sub> H <sub>10</sub>	0.0025	0.0042	0.0057	0.0092	0.0157	0.0289	0.0483	0.0621	0.0574	0.0392	0.0160	0	0
cyclopentadiene	0	0	0	0	0	0	0	0.0065	0.0528	0.0977	0.136	0.257	0.159
cyclopentene	0	0	0	0	0	0	0	0.0013	0.0057	0.0061	0.0059	0.0074	0.0035
cyclopentane	0	0	0	0	0	0	0.0011	0.0027	0.0069	0.0079	0.0067	0.0060	0
benzene	0	0	0	0	0	0	0	0.0017	0.0305	0.0844	0.219	0.756	0.829
cyclohexadiene	0	0	0	0	0	0	0	0	0.0039	0.0049	0.0060	0.0104	0.0054
toluene	0	0	0	0	0	0	0	0	0.0021	0.0072	0.0181	0.0577	0.0507
styrene	0	0	0	0	0	0	0	0	0.0022	0.0037	0.0181	0.0260	
total	100.7	100.7	100.7	100.5	100.2	100.4	100.4	100.6	100.6	100.5	100.2	100.4	100.0
C <sub>out</sub> /C <sub>in</sub>	0.99	0.99	0.98	0.98	0.99	1.00	0.99	0.98	0.97	0.96	0.94	0.95	0.88
H <sub>out</sub> /H <sub>in</sub>	0.99	1.00	0.98	0.99	0.99	1.00	1.00	0.99	0.98	0.97	0.97	0.98	0.96

<sup>a</sup> Set 2: C<sub>2</sub>H<sub>6</sub>/N<sub>2</sub> = 50.2/49.8.

species formed at the highest temperatures. The GC/MS permits more unambiguous identification of the molecular weight growth species. In these experiments, the 5890 GC was set up such that the C<sub>2</sub> species were not detected and acetylene and ethylene were not separated on the Trace GC/MS. Thus, the reported C<sub>2</sub>H<sub>4</sub> mole fraction should be considered as the sum of C<sub>2</sub>H<sub>4</sub> and C<sub>2</sub>H<sub>2</sub>.

These experiments were then repeated (set 3) with the 5890 configured so as to separate C<sub>2</sub>H<sub>2</sub> from C<sub>2</sub>H<sub>4</sub> as well as to confirm the earlier data. These data are listed in Table 3. Although there are clear indications of increasing acetylene production at the higher temperatures, the variations in the measurements were much higher than those observed for other species, resulting in considerable uncertainties in the quantification. These uncertainties propagate into the observed mole fraction sum, which now begins to deviate at the highest temperatures where acetylene production is observed. These deviations suggest that perhaps the actual acetylene yield is somewhat higher than reported. The measured carbon and hydrogen balances are intermediate between those observed in sets 1 and 2.

Inspection of Figure 2 reveals many interesting features of the kinetics of ethane pyrolysis. Under the selected experimental conditions, virtually no ethane conversion is observed at 550 °C, while there is almost complete conversion at 850 °C. The decrease in the nitrogen mole fraction (not shown, but listed in Tables 1–3) signifies an increase in the number of moles as ethane reacts. The major products are ethylene and hydrogen, followed by methane. Molecular weight growth starts with the formation of small amounts of butane at 550 °C, followed by

propylene, propane, 1,3-butadiene, and 1-butene at 675 °C. Cyclopentane is produced at 700 °C, followed by 2-butene, cyclopentadiene, cyclopentene, and benzene at 725 °C. Cyclohexadiene and toluene are formed starting at 750 °C. Styrene first appears at 775 °C. At 800 °C, acetylene first appears, along with indene, naphthalene, and acenaphthalene. In general, the three sets of experiments yielded consistent results, with very good agreement for the major species. Where there are deviations for minor species, the trends with temperature are still similar.

Of interest is the observation that most C<sub>2</sub> to C<sub>5</sub> products, with the exception of the acetylene, allene, and propyne, all exhibit a pronounced peak in their concentration at temperatures between 725 and 800 °C, suggesting the importance of subsequent reactions. Similar behavior is observed for cyclohexadiene. In contrast, the production of benzene and the higher molecular weight species continues to increase over the entire temperature range. Note that the drop in ethylene mole fraction above 800 °C is ~3.4%, much larger than that for any other species. Considering this is equivalent to ~6.8% carbon atoms, the amount of this decrease is sufficient to account for all of the carbon (~6.3%) appearing in the species from benzene to acenaphthalene. We can think of ethylene as playing the same role in promoting molecular weight growth in this low temperature regime that acetylene plays at higher temperatures in terms of soot production. At these relatively low temperatures, the rate of acetylene production is too low for it to be a major contributor to molecular weight growth. Note it only begins to form at 800 °C. Following ethylene, the olefins with the next two highest concentrations are propylene and 1,3-butadiene. These also peak near 800 °C and

**Table 3.** Experimental Data Obtained from Ethane Pyrolysis<sup>a</sup>

species	average experimentally observed mole %									
	550 °C	600 °C	650 °C	700 °C	750 °C	800 °C <sup>b</sup>	825 °C <sup>c</sup>	850 °C <sup>c</sup>	800 °C <sup>d</sup>	850 °C <sup>d</sup>
H <sub>2</sub>	0	0.26	1.95	8.3	19.6	28.2	28.4	30.0	26.0	29.3
N <sub>2</sub> /He	51.1	50.6	50.3	47.3	41.4	35.4	34.8	33.7	35.7	33.7
CH <sub>4</sub> (trace)	0	0	0.03	0.26	1.66	4.82	7.47	9.77	4.96	9.82
C <sub>2</sub> H <sub>6</sub>	48.5	47.9	45.3	36.1	19.2	6.7	3.7	2.2	6.8	2.2
C <sub>2</sub> H <sub>4</sub>	0.03	0.31	2.01	8.54	19.2	24.1	22.9	20.2	24.1	20.2
C <sub>2</sub> H <sub>2</sub>	0	0	0	0	0.00	0.147	0.313	0.572	0.149	0.489
C <sub>3</sub> H <sub>6</sub>	0	0	0	0.03	0.20	0.239	0.213	0.159	0.254	0.159
C <sub>3</sub> H <sub>8</sub>	0	0	0	0	0.0172	0.0118	0.0060	0.0031	0.0137	0.0037
allene	0	0	0	0	0.00	0.0065	0.0110	0.0133	0.0070	0.0130
propyne	0	0	0	0	0	0.0028	0.0041	0.0045	0.0040	0.0044
1,3-C <sub>4</sub> H <sub>6</sub>	0	0	0	0.0125	0.154	0.334	0.373	0.319	0.365	0.309
1-C <sub>4</sub> H <sub>8</sub>	0	0	0	0.0074	0.0182	0.0152	0.0086	0.0041	0.0174	0.0041
2-C <sub>4</sub> H <sub>8</sub>	0	0	0	0	0.0098	0.0158	0.0089	0.0058	0.0088	0.0057
n-C <sub>4</sub> H <sub>10</sub>	0	0	0.0113	0.0471	0.0429	0.0125	0.0103	0.0127	0.0086	0.0126
cyclopentadiene	0	0	0	0	0.0349	0.115	0.117	0.102	0.105	0.099
cyclopentene	0	0	0	0	0.0021	0.0059	0.0017	0.0015	0.0021	0.0014
cyclopentane	0	0	0	0	0.0034	0.0031	0.0023	0.0015	0.0029	0.0015
benzene	0	0	0	0	0.0147	0.168	0.510	0.803	0.240	0.763
cyclohexadiene	0	0	0	0	0.0001	0.0073	0.0051	0.0033	0.0000	0.0032
toluene	0	0	0	0	0.0084	0.0156	0.0388	0.0489	0.0192	0.0459
styrene	0	0	0	0	0	0.0051	0.0243	0.0392	0.0089	0.0355
indene	0	0	0	0	0	0.0020	0.0081	0.0141	0.0024	0.0115
naphthalene	0	0	0	0	0	0.0038	0.0242	0.0572	0.0046	0.0421
acenaphthalene	0	0	0	0	0	0	0.0015	0.0025	0.0000	0.0013
total	99.6	99.2	99.5	100.5	101.5	100.3	99.0	98.1	98.8	97.3
C <sub>out</sub> /C <sub>in</sub>	1.00	1.00	0.99	1.00	1.02	0.99	0.95	0.93	0.96	0.90
H <sub>out</sub> /H <sub>in</sub>	1.00	1.00	0.99	1.00	1.02	1.01	0.97	0.98	0.96	0.95

<sup>a</sup> Set 3: C<sub>2</sub>H<sub>6</sub>/N<sub>2</sub> = 48.4/50.9. <sup>b</sup> With initial N<sub>2</sub>/C<sub>2</sub>H<sub>6</sub> = 49.4/50.1. <sup>c</sup> With initial N<sub>2</sub>/C<sub>2</sub>H<sub>6</sub> = 49.2/50.8. <sup>d</sup> With He as the bath gas, initial He/C<sub>2</sub>H<sub>6</sub> = 48.9/51.3.

subsequently decay to form higher molecular weight species. Thus, olefins are observed to play the dominant role in molecular weight growth kinetics in this relatively low temperature environment.

The predictions using the original model are compared to the experimental data in Figure 3. Comparisons are only made for species up to C<sub>6</sub>, because this model does not include a complete set of reactions for species above C<sub>6</sub>. Over the entire temperature range, the model does a very good job in predicting the ethane conversion and production of hydrogen and ethylene. The mole fraction of methane is underpredicted at temperatures above 700 °C. Acetylene is underpredicted, but the model reproduces the observed very rapid increase in concentration with temperature; given the uncertainty in the acetylene calibrations, there might not be a significant problem. The propylene mole fraction profile is reasonable, given the data scatter. Predicted propane and butane yields display the proper temperature dependence, but both are underpredicted. The calculated allene mole fraction is in reasonable agreement, given the scatter in the data, but propyne yields are significantly over predicted. Although all three C<sub>4</sub> olefins are significantly over predicted, the model captures the effect of temperature. The cyclopentadiene predictions show a much stronger temperature dependence than observed. The cyclopentene results are similar to the C<sub>4</sub> olefins in terms of the proper temperature dependence, but the mole fractions are also significantly overpredicted. The

cyclopentane yields are substantially underpredicted. The cyclohexadiene yields are underpredicted, but the effect of temperature is similar to that observed. The benzene predictions properly describe the onset temperature, but then underestimate the impact of increasing temperature.

Although the ability of this unadjusted mechanism to quantitatively describe the ethane conversion and the major products is encouraging, it is clear that mechanism improvements are needed to properly account for the series of reactions that ultimately lead to molecular weight growth. One troublesome aspect involves the mismatch in the predicted temperature dependence of both benzene and cyclopentadiene mole fractions. This is likely related to the systematic overprediction of the olefinic intermediates, especially 1,3-butadiene, suggesting fundamental problems with the mechanism. Thus, we performed both a rate and a sensitivity analysis to identify the reactions that need additional analysis to improve the model. We are particularly interested to see if the remaining discrepancies can be satisfactorily addressed by an improved understanding of existing reactions in the mechanism or whether it might be necessary to consider additional reactions.

**4.2. Sensitivity and Rate of Production Analysis.** The results of the sensitivity analysis obtained with CHEMKIN PRO for all of the species observed with six or fewer carbon atoms, performed for

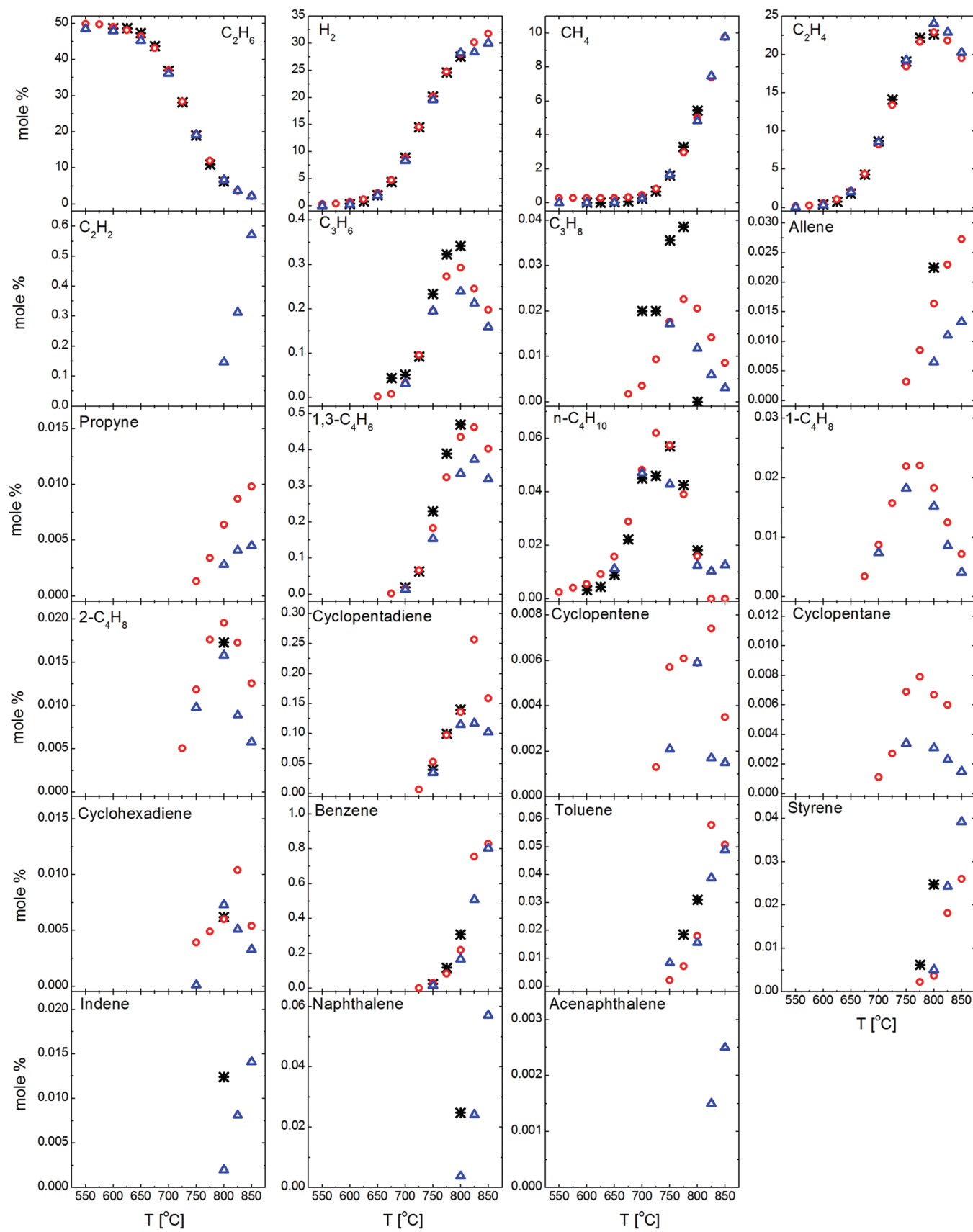


**Figure 2.** Experimental product distribution in the pyrolysis of  $\sim 50/50$  ethane/ $N_2$  mixtures at  $P = 0.8$  atm,  $\tau \approx 5$  s. \* = set 1, ○ = set 2, △ = set 3. See text and Tables 1–3 for details.

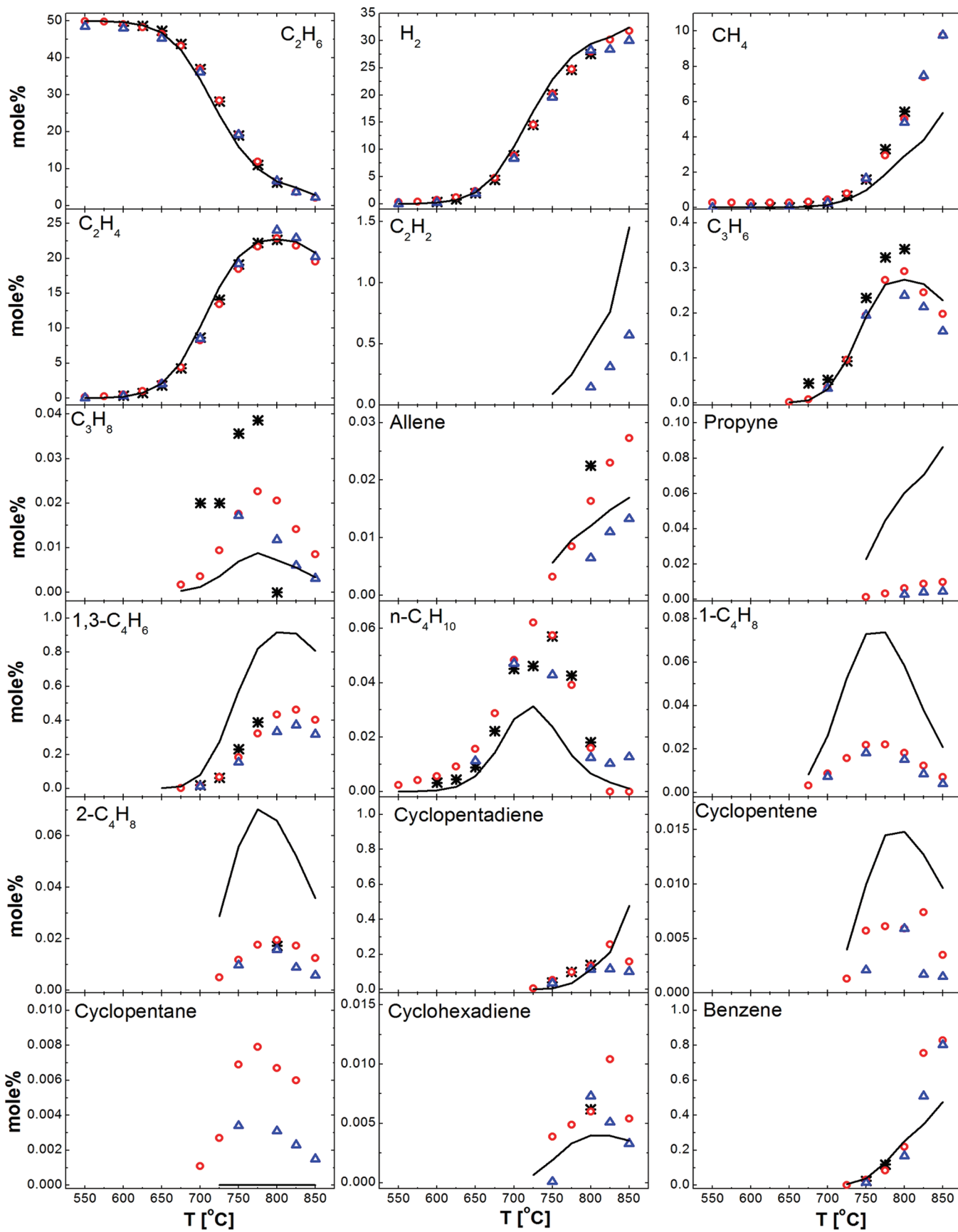


**Figure 3.** Comparison of experimental species mole fractions (in percent) with modeling predictions. Symbols, experimental data; solid lines, modeling results with the “original” mechanism (see text).

**Table 4.** Normalized Sensitivity Coefficients Calculated at the End of the Hot Zone of the Reactor at 750 °C for Species with Three or Less Carbon Atoms

reactions	species								
	C <sub>2</sub> H <sub>6</sub>	H <sub>2</sub>	C <sub>2</sub> H <sub>4</sub>	CH <sub>4</sub>	C <sub>2</sub> H <sub>2</sub>	C <sub>3</sub> H <sub>6</sub>	C <sub>3</sub> H <sub>8</sub>	allene	propyne
(1) C <sub>2</sub> H <sub>6</sub> + H ⇌ C <sub>2</sub> H <sub>5</sub> + H <sub>2</sub>	-0.28	0.17	0.16	-0.13	-0.10	0.16		0.20	
(2) H + C <sub>2</sub> H <sub>4</sub> (+M) ⇌ C <sub>2</sub> H <sub>5</sub> (+M)	-0.17	0.11			0.24			0.17	0.20
(3) 2CH <sub>3</sub> (+M) ⇌ C <sub>2</sub> H <sub>6</sub> (+M)	-0.18			0.69	0.42	0.41	0.59	0.36	0.41
(4) 2C <sub>2</sub> H <sub>5</sub> (+M) ⇌ CCCC(+M)	0.13				-0.31		-0.15	-0.22	-0.28
(5) C <sub>2</sub> H <sub>4</sub> + H ⇌ C <sub>2</sub> H <sub>3</sub> + H <sub>2</sub>					0.30			0.21	0.23
(6) C <sub>2</sub> H <sub>6</sub> + CH <sub>3</sub> ⇌ C <sub>2</sub> H <sub>5</sub> + CH <sub>4</sub>							-0.20		
(7) CCC + H ⇌ CCC <sup>*</sup> + H <sub>2</sub>							-0.17		
(8) CH <sub>4</sub> + H ⇌ CH <sub>3</sub> + H <sub>2</sub>							-0.21		
(15) C=CC <sup>*</sup> + C <sub>2</sub> H <sub>5</sub> ⇌ C=C=C + C <sub>2</sub> H <sub>6</sub>								0.10	
(16) CH <sub>3</sub> + C <sub>2</sub> H <sub>5</sub> (+M) ⇌ CCC(+M)								0.46	
(17) C=CCC(+M) ⇌ C=CC <sup>*</sup> + CH <sub>3</sub> (+M)				0.11	0.12	0.18	0.20		
(18) H + C <sub>2</sub> H <sub>2</sub> (+M) ⇌ C <sub>2</sub> H <sub>3</sub> (+M)					0.41				
(19) CH <sub>3</sub> + C <sub>2</sub> H <sub>4</sub> ⇌ H + C=CC							-0.23		
(20) C <sub>2</sub> H <sub>4</sub> + C <sub>2</sub> H <sub>5</sub> ⇌ C=CCC + H							0.16	0.14	0.13
(23) CCC <sup>*</sup> =C ⇌ CH <sub>3</sub> + C=C=C									0.13
(24) CC=CC <sup>*</sup> ⇌ C≡CC + CH <sub>3</sub>									0.29

**Table 5.** Normalized Sensitivity Coefficients Calculated at the End of the Hot Zone of the Reactor at 750 °C for Species with Four or More Carbon Atoms

reaction	species								
	1,3-butadiene	C <sub>4</sub> H <sub>10</sub>	1-butene	2-butene	1,3-cyclopentadiene	cyclopentene	cyclopentane	1,3-cyclohexadiene	benzene
(1) C <sub>2</sub> H <sub>6</sub> + H ⇌ C <sub>2</sub> H <sub>5</sub> + H <sub>2</sub>	0.24	0.19	0.20	0.20	-0.21	0.33	0.38	0.30	
(2) H + C <sub>2</sub> H <sub>4</sub> (+M) ⇌ C <sub>2</sub> H <sub>5</sub> (+M)	0.21	-0.29		0.21	0.47	0.17	0.30	0.30	0.47
(3) 2CH <sub>3</sub> (+M) ⇌ C <sub>2</sub> H <sub>6</sub> (+M)	0.29	0.19	0.20	0.29	0.89	0.36	0.53	0.39	0.75
(4) 2C <sub>2</sub> H <sub>5</sub> (+M) ⇌ CCCC(+M)	-0.23	0.75	-0.15	-0.20	-0.65	-0.16	-0.29	-0.30	-0.58
(5) C <sub>2</sub> H <sub>4</sub> + H ⇌ C <sub>2</sub> H <sub>3</sub> + H <sub>2</sub>	0.32	-0.09	0.09	0.25	0.49	0.10		0.44	0.53
(9) CCCC + H ⇌ CCC <sup>*</sup> C + H <sub>2</sub>		-0.60							
(10) CCCC + H ⇌ CCCC <sup>*</sup> + H <sub>2</sub>		-0.15							
(11) CyC <sub>5</sub> H <sub>10</sub> + H ⇌ CyC <sub>5</sub> H <sub>9</sub> <sup>*</sup> + H <sub>2</sub>							0.19		
(12) CHD13 + H ⇌ CyC <sub>6</sub> H <sub>7</sub> + H <sub>2</sub>								-0.62	
(13) CC=CC + C <sub>2</sub> H <sub>5</sub> ⇌ CC=CC <sup>*</sup> + C <sub>2</sub> H <sub>6</sub>				0.13					
(14) CyC <sub>5</sub> H <sub>10</sub> + C <sub>2</sub> H <sub>3</sub> ⇌ CyC <sub>5</sub> H <sub>9</sub> <sup>*</sup> + C <sub>2</sub> H <sub>4</sub>							0.38		
(17) C=CCC(+M) ⇌ C=CC <sup>*</sup> + CH <sub>3</sub> (+M)			-0.15			0.32	0.38		
(18) H + C <sub>2</sub> H <sub>2</sub> (+M) ⇌ C <sub>2</sub> H <sub>3</sub> (+M)				0.38					
(20) C <sub>2</sub> H <sub>4</sub> + C <sub>2</sub> H <sub>5</sub> ⇌ C=CCC + H		0.32				0.19	0.22		
(21) CCC <sup>*</sup> C ⇌ CC=CC + H			-0.19						
(22) CCC <sup>*</sup> C ⇌ CH <sub>3</sub> + C=CC			-0.12						
(25) C <sub>2</sub> H <sub>3</sub> + C=CC=C ⇌ C=CCC <sup>*</sup> C=C							0.34	0.38	
(26) C=CC <sup>*</sup> + C <sub>2</sub> H <sub>4</sub> ⇌ CyC <sub>5</sub> H <sub>8</sub> + H				0.14					

the 750 °C case at the end of the hot zone (corresponding to the reactor distance around 24 cm in Figure 1), are shown in Tables 4 and 5. The normalized sensitivity coefficient is the ratio of the relative change in the mole fraction of a species at a specified time to the relative change in a specific rate constant. Entries are only included if the normalized sensitivity coefficient is greater than 0.10. It is evident that a small number of reactions dominate the kinetics. Note that only four reactions exhibit significant sensitivity for the major species ethane, hydrogen, and ethylene that are accurately

predicted by the original model:

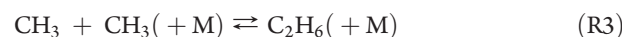
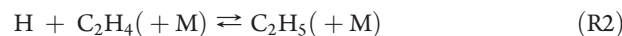
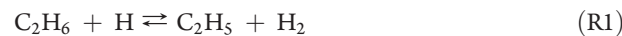


**Table 6.** Rate Constants for the Hydrogen Abstraction with Significant Normalized Sensitivity Coefficients<sup>a</sup>

reaction	<i>A</i>	<i>n</i>	<i>E</i>	<i>k</i> (1000 K)
(1) $\text{C}_2\text{H}_6 + \text{H} \rightleftharpoons \text{C}_2\text{H}_5 + \text{H}_2$	$1.07 \times 10^8$	1.95	8170	$1.24 \times 10^{12}$
(5) $\text{C}_2\text{H}_4 + \text{H} \rightleftharpoons \text{C}_2\text{H}_3 + \text{H}_2$	$8.30 \times 10^7$	2.00	12 800	$1.32 \times 10^{11}$
(6) $\text{C}_2\text{H}_6 + \text{CH}_3 \rightleftharpoons \text{C}_2\text{H}_5 + \text{CH}_4$	$1.90 \times 10^3$	2.98	10 800	$7.21 \times 10^9$
(7) $\text{CCC} + \text{H} \rightleftharpoons \text{CCC}^\bullet + \text{H}_2$	$1.01 \times 10^8$	1.96	8130	$1.28 \times 10^{12}$
(8) $\text{CH}_4 + \text{H} \rightleftharpoons \text{CH}_3 + \text{H}_2$	$3.00 \times 10^7$	2.07	11 200	$1.73 \times 10^{11}$
(9) $\text{CCCC} + \text{H} \rightleftharpoons \text{CCCC}^\bullet + \text{H}_2$	$2.11 \times 10^8$	1.82	5710	$3.44 \times 10^{12}$
(10) $\text{CCCC} + \text{H} \rightleftharpoons \text{CCCC}^\bullet + \text{H}_2$	$1.09 \times 10^8$	1.94	8300	$1.10 \times 10^{12}$
(11) $\text{CyC}_5\text{H}_{10} + \text{H} \rightleftharpoons \text{CyC}_5\text{H}_9^\bullet + \text{H}_2$	$1.76 \times 10^7$	2.00	4600	$1.74 \times 10^{12}$
(12) $\text{CHD13} + \text{H} \rightleftharpoons \text{CyC}_6\text{H}_7 + \text{H}_2$	$6.16 \times 10^6$	2.23	-460	$3.80 \times 10^{13}$
(13) $\text{CC=CC} + \text{C}_2\text{H}_5 \rightleftharpoons \text{CC=CC}^\bullet + \text{C}_2\text{H}_6$	$7.99 \times 10^1$	3.21	7252	$8.86 \times 10^9$
(14) $\text{CyC}_5\text{H}_{10} + \text{C}_2\text{H}_3 \rightleftharpoons \text{CyC}_5\text{H}_9^\bullet + \text{C}_2\text{H}_4$	$3.21 \times 10^4$	2.77	3760	$9.88 \times 10^{11}$
(15) $\text{C=CC}^\bullet + \text{C}_2\text{H}_5 \rightleftharpoons \text{C=C=C} + \text{C}_2\text{H}_6$	$1.00 \times 10^{12}$	0	0	$1.00 \times 10^{12}$

<sup>a</sup>  $k = AT^n \exp(-E/RT) \text{ cm}^3 \text{ mol}^{-1} \text{ s}^{-1}$ ,  $E$  in kcal/mol.

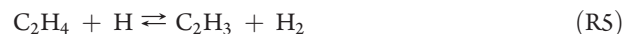
The high sensitivity of these reactions is consistent with the usual picture of hydrocarbon pyrolysis. Pyrolysis is initiated by dissociation of the parent (reverse of (R3)) to form radicals (initially  $\text{CH}_3$  but then H becomes more important) that can then abstract from the parent (R1), forming ethyl that can recombine in a termination reaction (R4) or undergo  $\beta$ -scission to form ethylene and H atoms (reverse of (R2)) to continue the chain.

The rate constant for (R1) is based on our CBS-QB3 calculations.<sup>19</sup> This value at 1000 K is only 14% larger than the value recommended in the Baulch review.<sup>25</sup> The  $\beta$ -scission of ethyl, (R2), has been considered by many investigators. In the present work, the high-pressure rate constant and its pressure dependence were taken from the analysis of Miller and Klippenstein.<sup>26</sup> This high-pressure value is similar (larger by a factor of 1.2) to the value recommended by Baulch et al.<sup>27</sup> Ethane dissociation to two methyl radicals, (R3), is a pressure-dependent reaction and has been studied extensively. The high-pressure rate constant of ethane dissociation measured in shock tube experiments by Oehlschlaeger et al.<sup>5</sup> was used in this work. This value was used as the input to our QRRK/MSC calculations to obtain the pressure-dependent values used in the mechanism. The high-pressure rate constant of (R4) was taken from the Klippenstein et al.<sup>28</sup> analysis using variational transition state theory. The temperature and pressure-dependent rate constants for *n*-butane dissociation were then obtained with the QRRK/MSC approach. The fact that the mechanism, using rate constants consistent with the well-documented literature values for the most sensitive reactions, accurately describes the kinetic data for the three major species is very encouraging. We can assume that these rate constants are appropriate, and we do not consider any adjustments in these assignments.

When considering the sensitivity analysis for the minor species, we will focus on reactions other than (R1)–(R4) for the reasons discussed above. The other reactions with significant coefficients are included in Table 4 (for species with less than four carbon atoms) and Table 5 (for species with four or more carbon atoms). It is noteworthy that a total of only 26 reactions can account for most of the variation in concentrations of all of the species predicted by the mechanism. Of these, many only affect a few species. We will consider these rate constant assignments in terms of three sets of reactions: (1) a series of hydrogen abstraction reactions (including a disproportionation reaction), (2) the pressure-dependent dissociation of the stable species 1-butene and propane, and

(3) pressure-dependent radical addition reactions that are expected to account for most of the molecular weight growth kinetics.

*Hydrogen Abstraction Reactions.* The rate constants are listed in Table 6. The abstraction reaction with the most pervasive influence is

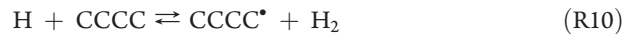
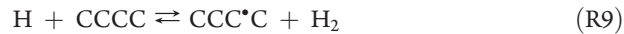


Our value is based on a CBS-QB3 calculation. At 1000 K, it is a factor of ~20% higher than the estimate of Tsang,<sup>29</sup> a factor of ~2 larger than the calculated value of Huynh et al.,<sup>30</sup> and 7% higher than the extrapolated value from molecular-beam mass spectrometry measurement of Bhargava and Westmoreland.<sup>31</sup> Given the spread of the rate constants, we see little justification to change this value.

All of the other hydrogen abstraction reactions only affect the prediction of a single species. The rate constant for the reaction



is based on a CBS-QB3 calculation. It is in very good agreement (within 15% at 1000 K) with the values recommended by both Tsang<sup>29</sup> and Baulch et al.<sup>32</sup> CBS-QB3 values were also used for the reactions:



(In the above equations and later in the text, the hydrogen atoms are sometimes omitted for clarity.) This  $k_7$  value is 30% lower than the Tsang estimate<sup>33</sup> at 1000 K. The value for  $k_8$  is bracketed by the values cited in the reviews of Baulch et al.<sup>32</sup> and Sutherland et al.<sup>34</sup> Both  $k_9$  and  $k_{10}$  are within ~5% of the value measured by Baldwin and Walker<sup>35</sup> and ~20% lower than that used by Curran.<sup>36</sup>

The value used for  $k_{11}$  is based on a CBS-QB3 calculation:

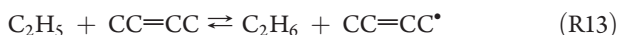


This relatively low value reflects an unusually low *A*-factor calculated for this reaction, as compared to other cycloalkanes.<sup>19</sup> Another unusual feature of this reaction is that the bond energy

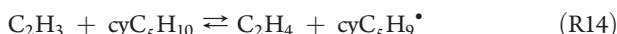
in cyclopentane is calculated to be 3–4 kcal/mol lower than either cyclobutane or cyclohexane. Abstraction from 1,3-cyclohexadiene is expected to be fast because a highly stable radical is formed:



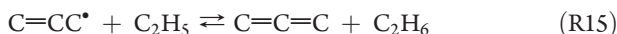
The value used is an estimate based upon analogies to other abstraction reactions that form resonantly stabilized radicals. Similarly, an estimate was used for ethyl abstraction from 2-butene:



The rate constant for vinyl abstraction from cyclopentane:

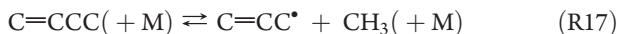


is an estimate based upon the assumption that the abstraction would be analogous to abstraction from a linear alkane. We saw above that this assumption is not appropriate for abstraction by H-atoms, so there remains considerable uncertainty regarding the value used for  $k_{14}$ . However, the sensitivity analysis indicates that this reaction has a major impact only on cyclopentane production and this is a very minor product and is not expected to play any significant role in molecular weight growth. Finally, we note the disproportionation reaction:



affects allene production. We assign  $k_{15} = 1.0 \times 10^{12} \text{ cm}^3 \text{ mol}^{-1} \text{ s}^{-1}$ , a value slightly higher than that suggested by Tsang.<sup>37</sup>

*Pressure-Dependent Dissociation Reactions.* In addition to dissociation of ethane and butane discussed above, two other dissociation reactions are identified in the sensitivity analysis:



The high-pressure rate constant of propane dissociation was based on the shock tube measurements by Oehlschlaeger et al.,<sup>5</sup> and the pressure dependence was calculated as described above for ethane dissociation. The high-pressure value for 1-butene dissociation was determined on the basis of an estimate of the recombination rate constant,  $k_{-17} \approx 2.8 \times 10^{13} \text{ cm}^3 \text{ mol}^{-1} \text{ s}^{-1}$ , and the equilibrium constant. The pressure dependence was then computed in the usual way. The pressure-dependent rate constants are included in the Supporting Information.

**4.3. Analysis of Pressure-Dependent Radical Addition Reactions.** We conclude from this sensitivity analysis that it is unlikely that any reasonable adjustments to the rate constants of the reactions described above will lead to significant changes in the predictions for most species. Generally these rate constants are quite well-defined, and the changes required to improve the predictions for the troublesome species would be too large to justify. We then considered the remaining sensitive reactions, those involving radical addition. In general, the rate constants for these reactions, even at the high-pressure limit, are not as well-defined. One reason for this is that such measurements need to properly account for the competing radical abstraction reactions. In the original mechanism, the rate constants of these reactions were based on a chemical activation analysis using approximate empirical potential energy surfaces. This has the potential to introduce some uncertainties. To improve this situation, we initiated a series of electronic structure calculations to characterize these potential energy surfaces. All calculations were performed with

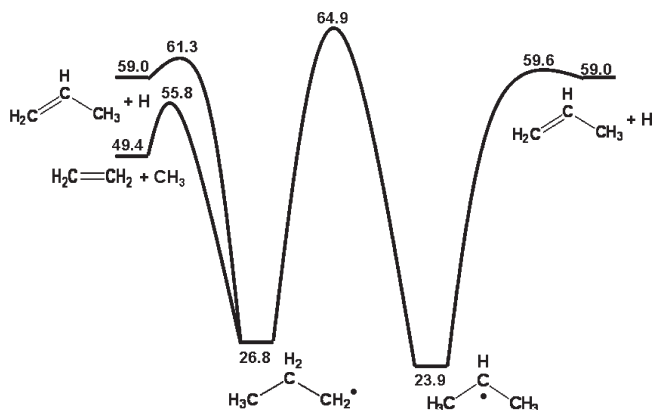
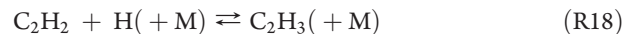


Figure 4. Potential energy surface for  $\text{C}_3\text{H}_7$  calculated at the CBS-QB3//QCISD/6-31G(D) level of theory, showing enthalpies in kcal/mol at 298 K.

the Gaussian 03 computational package.<sup>38</sup> Electronic energies were calculated either with the original or with a modified CBS-QB3 method. The original CBS-QB3 method optimizes the geometry and calculates the frequencies of a H/C species at the B3LYP/6-311G(2d,p) level, extrapolates the MP2 energy to the complete basis set energy limit, utilizing the asymptotic convergence of the correlation energy expanded in natural pair orbitals, and adds further corrections to obtain the CBS-QB3 energy. The frequencies are scaled by a factor of 0.99 prior to their use to calculate zero point energies (ZPE) and thermodynamic properties. The modified CBS-QB3 version also used in this work contains the same energy calculation steps, but it uses geometries and frequencies obtained at the QCISD/6-31G(d) level. This modified method, to which we will refer as CBS-QB3//QCISD/6-31G(d), uses the QCISD/6-31G(d) frequencies without further scaling. The high-pressure values obtained from this analysis were then used to calculate the pressure-dependent rate constants for the various channels. Because this work focuses on rate expressions, only relative energies are needed, and no attempts were made to improve on absolute heat of formation values, for example, by applying bond additivity corrections. Because this might lead to slight differences between the enthalpies and entropies calculated in this way and those obtained for other species via group additivity, we accounted for these differences by writing all of the reactions considered on the PES surfaces irreversibly. Thus, we separately considered every entrance channel to the PES and used forward rate constants in the mechanism. Similarly, we considered the unimolecular reactions of each stabilized adduct separately. This approach preserved internal consistency within these reactions while allowing this subset to be combined into a larger mechanism that treated the other reactions in the normal reversible manner.

The pressure dependence of



has been examined in detail by Miller and Klippenstein,<sup>26</sup> and we have used their values. Because the pressure dependence was reported in a form that is not compatible with CHEMKIN PRO, we refitted their values to modified Arrhenius expressions at several pressures and used those in our mechanism.

*Potential Energy Surface for  $\text{C}_3\text{H}_7$ .* The PES is shown in Figure 4. Three entrance channels are shown. As discussed above, the analysis considered each of these entrance channels individually. A rate

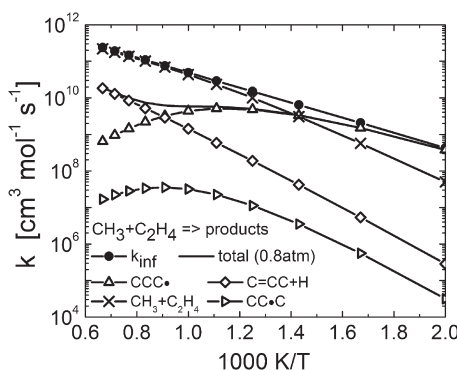
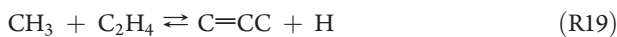


**Figure 5.** Calculated apparent rate constants at 0.8 atm of the product channels resulting from methyl addition to ethylene. (Most H atoms in the species names are omitted for clarity.)

analysis (with the original mechanism) at 750 °C showed that the major production reaction for *n*-propyl was H addition to the central carbon in propylene, and the primary decay pathway was formation of methyl and ethylene. One reason this pathway “runs backward” can be seen by inspection of the PES where the exit channel to form methyl + ethylene is significantly lower than that for H + propylene. Methyl addition to ethylene leads either to formation of the stabilized *n*-propyl radical or to redissociation out the entrance channel because the barriers to either H-atom elimination or isomerization to form isopropyl are higher. The subsequent dissociation of the stabilized *n*-propyl will also lead to methyl + ethylene. Thus, this reaction can be considered partially equilibrated. Conversely, H addition to propylene to form *n*-propyl is essentially irreversible because production of ethylene + methyl dominates, either directly from the energized adduct or later as the stabilized adduct dissociates. Thus, the reactions on the *n*-propyl PES effectively reverse molecular weight growth. The rate analysis for isopropyl showed formation via H addition to the terminal carbon was by far the dominant reaction. The energized adduct was then either collisionally stabilized to form isopropyl or dissociated to form methyl and ethylene, indicating that some of the energized complexes had enough internal energy to surmount the isomerization barrier.

Our calculated value for the high-pressure rate constant for *n*-propyl dissociation to methyl + ethylene is ~2.6 times larger at 1000 K than that computed by Zheng and Blowers<sup>39</sup> and ~3.2 times larger than that used by Curran.<sup>36</sup> This difference is due to a higher value for the *A*-factor; all of the activation energies are within 0.5 kcal/mol. Our value for *n*-propyl dissociation to propylene + H is a factor of ~2.8 higher than the value used by Curran;<sup>36</sup> again, the difference is due to the *A*-factor. The calculated high-pressure rate constant of  $\beta$ -scission of isopropyl to H + propylene is only ~10% lower at 1000 K than the measurements of Seakins et al.<sup>40</sup> and 1.6 times larger than the value provided by Curran.<sup>36</sup>

The temperature dependence of the apparent rate constants for the addition of CH<sub>3</sub> radicals to ethylene at 0.8 atm is shown in Figure 5. Formation of *n*-propyl dominates until ~600 K, at which point the reverse reaction becomes most important. Above 1000 K, formation of propylene + H begins to become significant:



The isomerization barrier is sufficiently high that very little isopropyl is formed. The mechanism also accounts for the subsequent reactions of the stabilized *n*-propyl radical. This is obtained

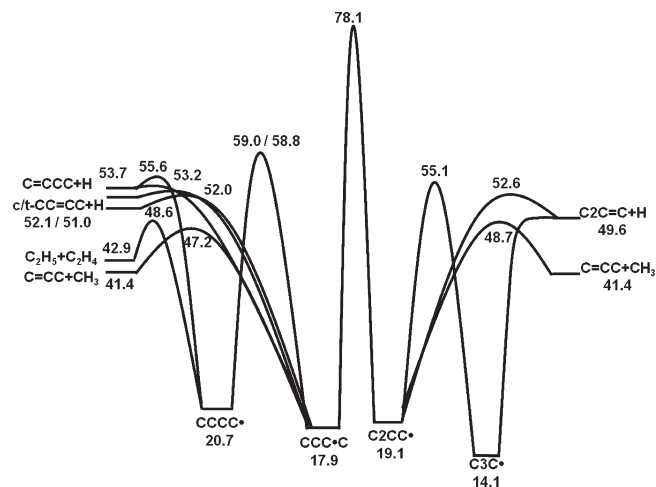
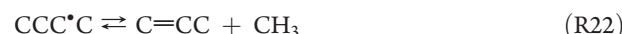


**Figure 6.** Potential energy surface for C<sub>4</sub>H<sub>9</sub> calculated at the CBS-QB3//QCISD/6-31G(d) level of theory, showing enthalpies in kcal/mol at 298K. (Most H atoms in the species names are omitted for clarity.)

by a similar QRRK/MSC analysis, but now using the thermal distribution function instead of the chemically activated one. An important result for this analysis is that the branching ratio for *n*-propyl  $\beta$ -scission to form methyl + ethylene versus H + propylene is 125 at 1000 K, whereas this ratio was only 18 using the earlier empirical potential energy surface.

*Potential Energy Surface for C<sub>4</sub>H<sub>9</sub>.* There are three reactions on this surface that appear in the sensitivity analysis:



This more complex surface is shown in Figure 6. It can be accessed by either methyl addition to propylene, ethyl addition to ethylene, or H addition to C<sub>4</sub> olefins. The high isomerization barrier separating the linear adducts from branched adducts effectively divides this surface into two subsets. As with the C<sub>3</sub>H<sub>7</sub> surface, the  $\beta$ -scission channels to form alkyl radicals are lower in energy than those forming H-atoms. The calculated rate constant for  $\beta$ -scission of *n*-butyl to form ethyl + ethylene is about a factor of 3 faster at 1000 K than that calculated by Zheng and Blowers.<sup>41</sup> This difference is due to a lower barrier of ~1.7 kcal/mol in the current work. Our value at 1000 K is ~2.2 times that used by Curran,<sup>36</sup> due to a 1 kcal/mol lower barrier and a slightly higher *A*-factor. However, our calculated value is over 7 times larger at 1000 K than the measurements of Knyazev et al.<sup>42</sup> The calculated high-pressure rate constant of *n*-butyl  $\beta$ -scission to form methyl + propylene is about a factor of 2 lower at 1000 K than reported by Curran<sup>36</sup> and Knyazev et al.<sup>42</sup> and a factor of 3 higher at 1000 K than the Tsang<sup>43</sup> value. The calculated rate constant of *s*-butyl  $\beta$ -scission to form methyl + propylene is very similar to the Curran<sup>36</sup> value at 1000 K, and about a factor of 2 higher than the measurements of Gang et al.<sup>44</sup> and of Knyazev et al.<sup>42</sup>

A rate analysis showed that *n*-butyl is produced by both the chemically activated ethyl + ethylene reaction and the abstraction from *n*-butane. Once formed, the primary unimolecular decay path is  $\beta$ -scission to ethyl + ethylene. Figure 7 shows the predicted

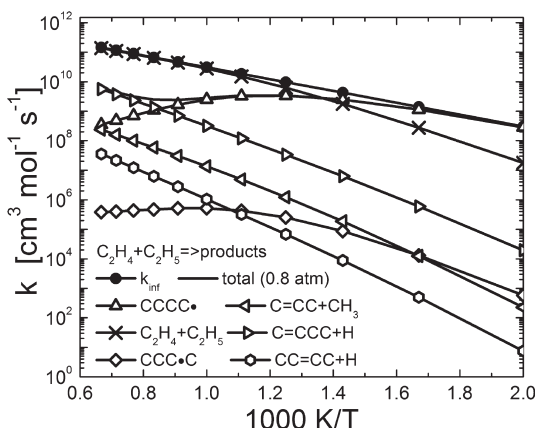


**Figure 7.** Calculated apparent rate constants at 0.8 atm of the product channels resulting from ethyl addition to ethylene. (Most H atoms in the species names are omitted for clarity.)

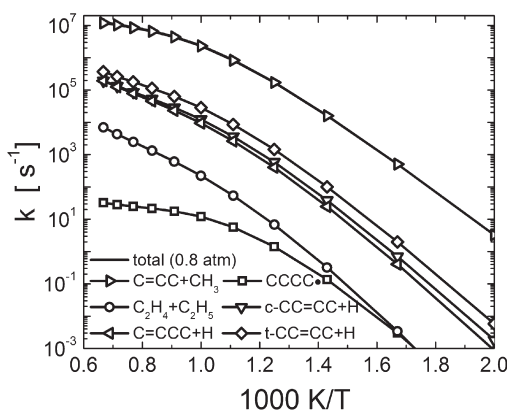
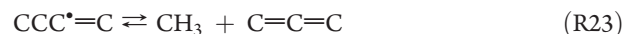


**Figure 8.** Predicted temperature dependence at 0.8 atm for the dissociation of the secondary butyl radical. (Most H atoms in the species names are omitted for clarity.)

rate constants at 0.8 atm when entering the PES via addition of ethyl to ethylene. Formation of stabilized *n*-butyl dominates at lower temperatures, followed by redissociation to reactants. Above 1000 K, formation of 1-butene + H from the chemically activated adduct begins to become important. Note the isomerization to *s*-butyl is insignificant, resulting from the combination of a high barrier and a low *A*-factor due to a tight transition state. As in the previous case, the subsequent thermalized unimolecular reactions of the stabilized *n*-butyl radical are an important part of the mechanism. Formation of *s*-butyl comes from chemically activated H addition to 1- or 2-butene (as well as via abstraction from butane). By far, the most dominant unimolecular decay channel of *s*-butyl is formation of methyl + propylene, as illustrated in Figure 8. The lower rate to form C<sub>4</sub> olefins + H is due to higher barriers. However, the competition between these pathways is important, as illustrated by the sensitivity analysis.

As can be seen in Figure 6, methyl addition to propylene can also lead to formation of isobutyl radicals. The rate analysis indicates that isobutyl is also produced by abstraction from isobutane or by H addition to isobutylene and that these radicals then  $\beta$ -scission to form propylene and methyl, another case of reversing molecular weight growth via H addition followed by methyl elimination. Hydrogen abstraction from isobutane can also lead to formation of *t*-butyl, which then forms isobutylene + H.

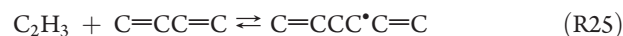
*Potential Energy Surface of C<sub>4</sub>H<sub>7</sub>.* Two reactions on the C<sub>4</sub>H<sub>7</sub> surface appear in the sensitivity analysis:



This surface is shown in Figure 9. Cyclic C<sub>4</sub>H<sub>7</sub> isomers were omitted due to their higher energies. The calculated barriers are generally within 1–3 kcal/mol of those calculated by Miller<sup>45</sup> by using the G03 method. This surface is qualitatively different from those discussed earlier in that several isomerization barriers are now lower than the C<sub>2</sub>H<sub>4</sub> + C<sub>2</sub>H<sub>3</sub> entrance channels and the channel forming H + 1,3-butadiene is also lower in energy. This difference is due to the relatively high heat of formation of vinyl, which increases the energy of the entrance channel, thereby leading to formation of a deeper adduct well. A rate analysis showed that the primary entrance channel to this surface is vinyl radical addition to ethylene. The initially formed C=CCC<sup>•</sup> radical may  $\beta$ -scission to form 1,3-butadiene + H, isomerize to form the resonantly stabilized C=CC<sup>•</sup>C radical, or isomerize to form CCC=C<sup>•</sup>. C=CC<sup>•</sup>C in turn can either isomerize to form CCC=C or CC=C<sup>•</sup>C, or it can  $\beta$ -scission to form 1,3-butadiene + H. CCC=C may then  $\beta$ -scission to allene + methyl (R23), while CC=C<sup>•</sup>C may  $\beta$ -scission to propyne + methyl. Note that (R24) reflects the combined isomerization– $\beta$ -scission pathway. Figure 10 shows the predicted apparent rate constants for these pathways at 0.8 atm. In contrast to the surfaces considered above, we see production of the stabilized adducts falling off more quickly as the temperature increases. In addition to redissociation to vinyl + ethylene, production of 1,3-butadiene + H becomes increasingly important at the higher temperatures. Formation of acetylene and ethyl is an order of magnitude slower than the 1,3-butadiene channel.

Several groups have investigated the reaction of vinyl radical and ethylene. Figure 11 compares these values with the results of this study. Fahr and Stein<sup>46</sup> used a very low pressure pyrolysis (VLPP) Knudsen cell flow reactor at 1023–1273 K and at low pressure between 1 and 10 mTorr. Shestov et al.<sup>47</sup> employed a tubular quartz flow reactor to study the reaction of C<sub>2</sub>H<sub>3</sub> + C<sub>2</sub>H<sub>4</sub> in the temperature range of 625–950 K. Ismail et al.<sup>48</sup> used a stainless steel flow reactor over a temperature region of 300–700 K and pressures of 20 and 133 mbar. Our calculated rate constant is about a factor of 3 larger than the measured values obtained by Ismail et al. Note both the observed data and the calculations show little effect of pressure on the overall rate constant. However, one expects a shift from some adduct formation in the lower temperature experiments to virtually none in the very low pressure, higher temperature experiments of Fahr and Stein.

*Potential Energy Surface of C<sub>6</sub>H<sub>9</sub>.* The sensitivity analysis illustrates the importance of the reaction:



for production of 1,3-cyclohexadiene and benzene. The potential importance of this reaction in terms of PAH growth was suggested by Cole et al.<sup>49</sup> Cavallotti et al.<sup>50</sup> investigated the addition of C<sub>2</sub>H<sub>3</sub> to 1,3-C<sub>4</sub>H<sub>6</sub> with the G2MP2 method coupled with QRRK theory. They found that it was more likely for C=CCC<sup>•</sup>C=C radical to isomerize to form an exocyclic five-member ring. The potential energy surface we used for this reaction is an extension of that recently calculated at the CBS-QB3 level by Sharma et al.<sup>14</sup> We added the vinyl addition to butadiene channel to their

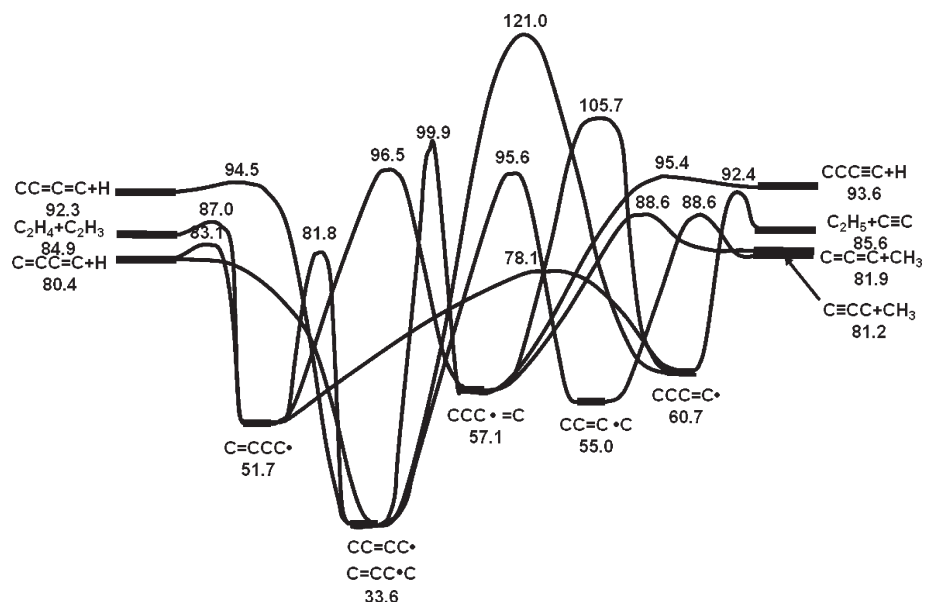


**Figure 9.** Potential energy surface for  $\text{C}_4\text{H}_7$  calculated at the CBS-QB3//QCISD/6-31G(d) level of theory showing enthalpies in kcal/mol at 298 K. (Most H atoms in the species names are omitted for clarity.)

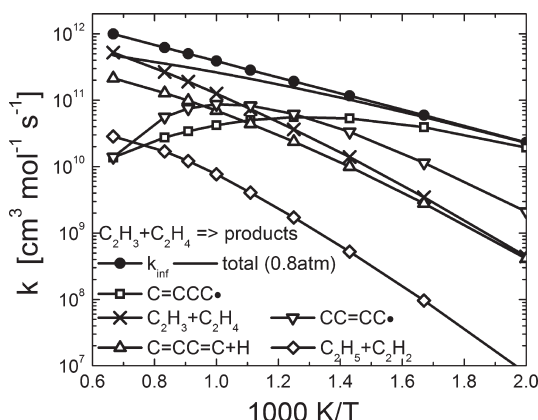


**Figure 10.** Predicted temperature dependence at 0.8 atm for the apparent rate constants for the product channels resulting from vinyl addition to ethylene. (Most H atoms in the species names are omitted for clarity.)

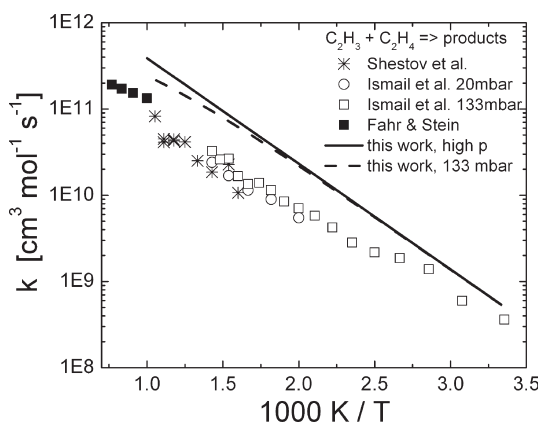


**Figure 11.** Comparison of measured overall rate constants for the reaction of vinyl with ethylene to that calculated in this study. Data: Shestov et al.,<sup>47</sup> Ismail et al.,<sup>48</sup> Fahr and Stein.<sup>46</sup>

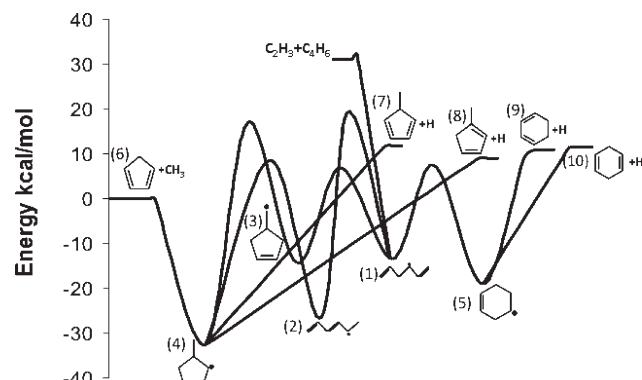


**Figure 12.** Modified version of the  $\text{C}_6\text{H}_9$  potential energy surface calculated by Sharma et al.<sup>14</sup> to include the addition of vinyl to 1,3-butadiene.

surface, as shown in Figure 12. The vinyl radical can react with 1,3-butadiene via a very low activation energy barrier, ~2 kcal/mol, to form the linear  $\text{C}_6\text{H}_9$  radical. This case represents a more extreme example of the shift in the PES discussed above for the  $\text{C}_4\text{H}_7$  surface. Not only is the entrance channel higher due to the vinyl reactant, but also the adduct well is lower due to formation of a resonantly stabilized species, dramatically tilting the distribution toward products, with redisassociation out the entrance channel not as important. This adduct can isomerize to form an endocyclic six-member ring 4-cyclohexenyl radical as well as an exocyclic five-member ring  $\text{cyC}_5\text{H}_7\text{CH}_2$  radical. The most stable product channel on the  $\text{C}_6\text{H}_9$  PES is methyl + cyclopentadiene, ~30 kcal/mol lower than vinyl + 1,3-butadiene. Formation of the six-membered ring 1,3-cyclohexadiene is ~12 kcal/mol higher than the cyclopentadiene channel, but still well below the energy of the entrance channel. The Sharma et al. PES has virtually no barriers (above the endothermicities) for formation of either the five- or the six-membered ring compounds. An earlier analysis by Saeys et al.<sup>51</sup> suggests that the barrier for methyl addition to a species that forms a resonantly stabilized radical is lower than that for formation of a nonresonantly stabilized radical but still on the

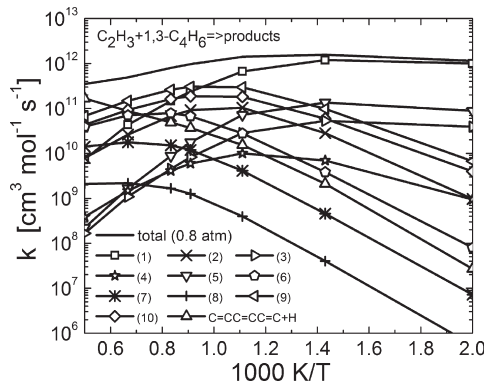


**Figure 13.** Predicted temperature dependence at 0.8 atm for the apparent rate constants for the product channels resulting from vinyl addition to 1,3-butadiene. (Notation: Product channel numbers correspond to the structures shown in Figure 12.)

order of  $\sim 4$  kcal/mol. We explored the sensitivity of the results to this barrier height and found virtually no impact.

Our previous rate constant for vinyl + 1,3-butadiene was estimated on the basis of vinyl + ethylene results from Fahr and Stein.<sup>46</sup> Our current high-pressure rate constant is about a factor of 23 faster than the original estimate at 1000 K. One reason for this difference might be the large difference in relative energy of the adduct to the reactants for these two reactions. For addition to ethylene, a primary radical is formed, while addition to 1,3-butadiene produced a resonantly stabilized secondary radical, leading to a much deeper well, as discussed above.

Figure 13 shows the predicted apparent rate constants for the multiple channels of this reaction at 0.8 atm. The deep well allows access to many exit channels. Near 800 °C, the dominant bimolecular products are the cyclohexadiene isomers and H atoms, followed by cyclopentadiene + methyl. Even with the deeper well, the reaction is well into the falloff regime, with much of the initially formed energized adduct going back out the entrance channel. Even though the exit channel to form cyclopentadiene plus methyl is significantly lower than those leading to the hexadiene isomers plus H, an additional isomerization step is required to form cyclopentadiene, and this leads to a slower rate of formation.

**4.4. Predictions with the Updated Mechanism.** The original mechanism was modified to include all of the reactions and associated pressure-dependent rate constants obtained from the radical addition reactions on the updated potential energy surfaces. This mechanism contained 229 species and 2234 reactions. Most of the large increase in the number of reactions is due to our approach to consider every entrance on each PES and to write these reactions irreversibly to properly represent the enthalpies and entropies calculated from the CBS-QB3//QCISD/6-31G-(d) results.

Figure 14 compares the updated predictions both to the data and to the original predictions. As expected from the sensitivity analysis, only slight changes are seen for ethane, hydrogen, and ethylene; both sets of predictions are in very good agreement with the data. Methane is significantly improved. A comparison of the impact of adding the updated reactions for one PES at a time to the mechanism shows little change in methane with the C<sub>3</sub>H<sub>7</sub> surface, but the other three are important. The propylene predictions are increased, but both sets are in reasonable agreement with the data. Reactions from all four surfaces have an impact on the mole fraction of this species. The predictions of 1,3-butadiene are significantly improved, mostly due to the C<sub>6</sub>H<sub>9</sub>

reactions. 2-Butene is also improved, again mostly due to the C<sub>6</sub>H<sub>9</sub> reactions. The predictions of both cyclohexadiene and benzene are improved.

The model seriously underestimates cyclopentane production. A rate analysis indicated that this species was produced via abstractions by the cyclopentyl radical. A possible reaction not included in the current model is the production of cyclopentane via recombination of two radicals that are present in large concentrations:

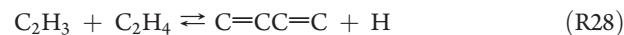


This reaction could occur via initial formation of an energized 1-pentene that then isomerizes via a biradical intermediate to cyclopentane.<sup>52</sup> However, an approximate chemical activation analysis treatment of this reaction, following the approach described by Sirjean et al.,<sup>52</sup> suggests this reaction will not be fast enough to contribute to cyclopentane production.

One interesting issue is the discrepancy in the temperature dependence of cyclopentadiene production. The fact that the data show a noticeable decline above 800 °C suggests subsequent reactions that are not included in the current model. We tested this hypothesis in several calculations where we included a reaction of this species with C<sub>2</sub>H<sub>3</sub>. Ignoring the complexities of the C<sub>7</sub>H<sub>8</sub> PES, we simply assumed the reaction proceeded irreversibly to form products with a rate constant similar to that used for vinyl addition to butadiene. The results are included in Figure 14. The preliminary results are encouraging in that it does appear that such a reaction has the potential to improve the predictions. Of course, a detailed analysis of this surface is required to confirm this suggestion; such an analysis is beyond the scope of this current work.

Overall, we find these comparisons encouraging. Clearly, some problems remain, but the substantial improvement in predictions of methane, 1,3-butadiene, 2-butene, cyclohexadiene, and benzene suggests that the updated rate constants derived from the analysis for the radical addition reactions are a step in the right direction toward developing a model to accurately predict molecular weight growth.

**4.5. Impact of Thermodynamic Properties.** Given the importance of the reaction sequence that produces 1,3-butadiene:



the predictions are surprisingly insensitive to these rate constants. A likely explanation for this is that the species in these reactions are partially equilibrated. To test this hypothesis, we compared the equilibrium constants for (R27) and (R29) to the predicted time-dependent mole fraction ratios of the species involved in these reactions and show the results in Figure 15. We see that the species concentrations involved in both reactions are very close to partial equilibrium at surprisingly early reaction times. Thus, the relative concentrations of these species are governed not by the kinetics, but by the thermodynamics that fixes the equilibrium constant. Interestingly, use of our group additivity thermo for these reactions causes a significant shift in the predicted ratios, again emphasizing the sensitivity to the thermodynamic values used. Similar considerations might also apply to other radical addition reactions. This result implies that to properly model molecular weight growth, an essential

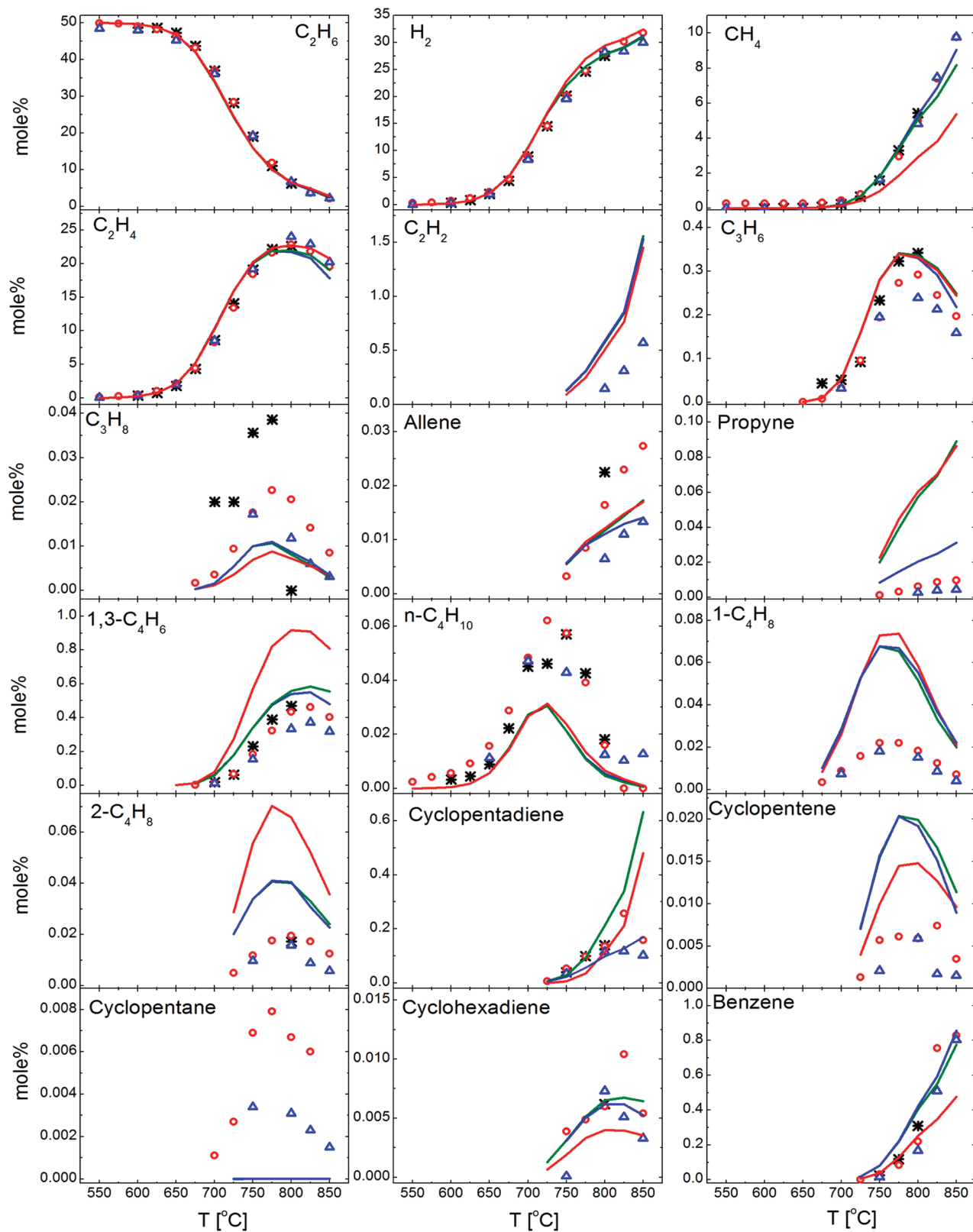


**Figure 14.** Comparison of model predictions to ethane pyrolysis data. Symbols: experimental data; green, predictions with updated mechanism; red, modeling results with original mechanism; blue, predicted results with added addition reaction of vinyl to cyclopentadiene (cf. text).

step is to carry the reaction sequence to the point where an especially stable species, for example, benzene, is produced so that the larger equilibrium constant associated with formation of this species can

“pull” the reaction toward completion. The added stability of aromatic compounds such as benzene is required to compensate for the entropy loss accompanying cyclization.

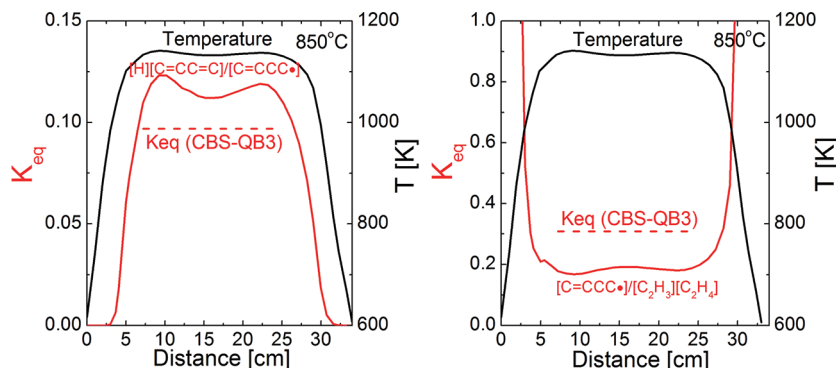
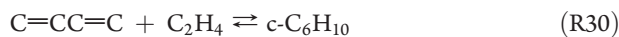


**Figure 15.** Comparison of the predicted distance-dependent concentration ratios to the equilibrium values predicted using the thermodynamic values obtained from the CBS-QB3 calculations.

**4.6. Other Potential Reactions of 1,3-Butadiene.** Given the critical role of 1,3-butadiene in molecular weight growth, as seen by the impact of the updated  $C_6H_9$  surface, we considered other potential reactions of this species that might be responsible for the formation of higher molecular weight growth species. Note in Figure 14 that, although the updated mechanism substantially improves the butadiene prediction, we still see a discrepancy at the highest temperatures where the observed decrease in the mole fraction is somewhat larger than predicted. In our model, the consumption reactions of 1,3-butadiene include thermal decomposition to form  $C_2H_4 + C_2H_2$ , hydrogen abstraction to form  $C_4H_5$  radicals, the Diels–Alder reaction of  $C_2H_4 + 1,3-C_4H_6$ , and radical additions with hydrogen, methyl, vinyl, and ethyl.

The thermal decomposition of 1,3-butadiene has been investigated extensively by many investigators.<sup>53–55</sup> The major pathway is isomerization to form 1,2- $C_4H_6$ , followed by subsequent decomposition to form ethylene and acetylene or methyl and propargyl. The submechanism of 1,3-butadiene decomposition developed by Hidaka et al.<sup>55</sup> based on a series set of shock tube experiments is used in our model. However, the relatively high barrier of  $\sim 72$  kcal/mol for this reaction, as calculated by Lee et al.,<sup>54</sup> means that this reaction is unlikely to be important at our experimental conditions.

Another reaction is the Diels–Alder cycloaddition:



The CBS-QB3 rate constant used in our mechanism is quite consistent with the literature value determined by Dayma et al.<sup>56</sup> However, this reaction does not contribute to butadiene decay because the equilibrium is shifted strongly toward the reactants near 800 °C.

Addition reactions with other radicals were also considered. Figure 16 shows the calculated radical concentrations at 800 °C. Ethyl is present in the largest concentration. Addition of ethyl to 1,3-butadiene has been considered in *n*-hexane pyrolysis.<sup>17</sup> The PES of  $C_6H_{11}$  has been calculated by Goldsmith et al.<sup>57</sup> using the G3 method. This PES is very complex; even a simplified one contains 14 isomers and a wide product distribution. Initially, an ethyl radical reacts with 1,3-butadiene via a low energy barrier to form 1-hexen-3-yl radical via (R31). After isomerization (R32), five- and six-membered rings can be formed via (R33) and (R34). Subsequent  $\beta$ -scission reactions produce either cyclohexene or methylcyclopentene.

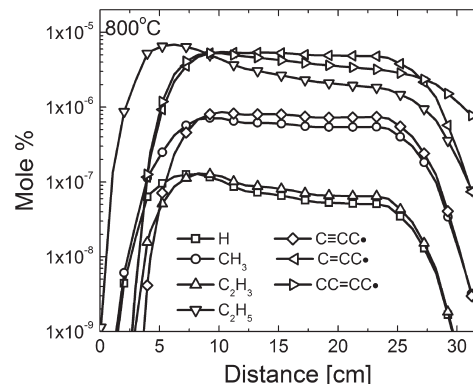
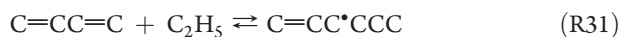
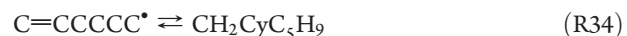
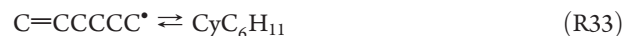


**Figure 16.** Calculated mole fractions of dominant radicals in ethane pyrolysis at 800 °C. (Most H atoms in the species names are omitted for clarity.)



The pressure-dependent rate constants of the major production channels for the reaction of vinyl radical with butenes were predicted using RRKM/ME calculations. On the basis of their calculations, it is found that the rate constants for the cyclic species formation were between 4 and 5 orders of magnitude lower than the highest rate constant for this system. Our QRRK analysis using their surface with ethyl + butadiene as the entrance channel predicted the dominant product channel to be the 1-hexen-3-yl radical with none of the cyclic isomers or the respective bimolecular products being formed at a significant rate. Thus, ethyl addition to 1,3-butadiene is not a significant route to production of stable higher molecular weight cyclic compounds under our conditions.

Although several resonantly stabilized radicals are predicted to be in relatively high concentrations, their addition reactions to butadiene are expected to be highly reversible because the well depth will be much lower, suggesting these reactions would be even less important than the ethyl addition case discussed above.

Methyl is also present in relatively high concentrations. This addition is included in the mechanism, but it does not contribute

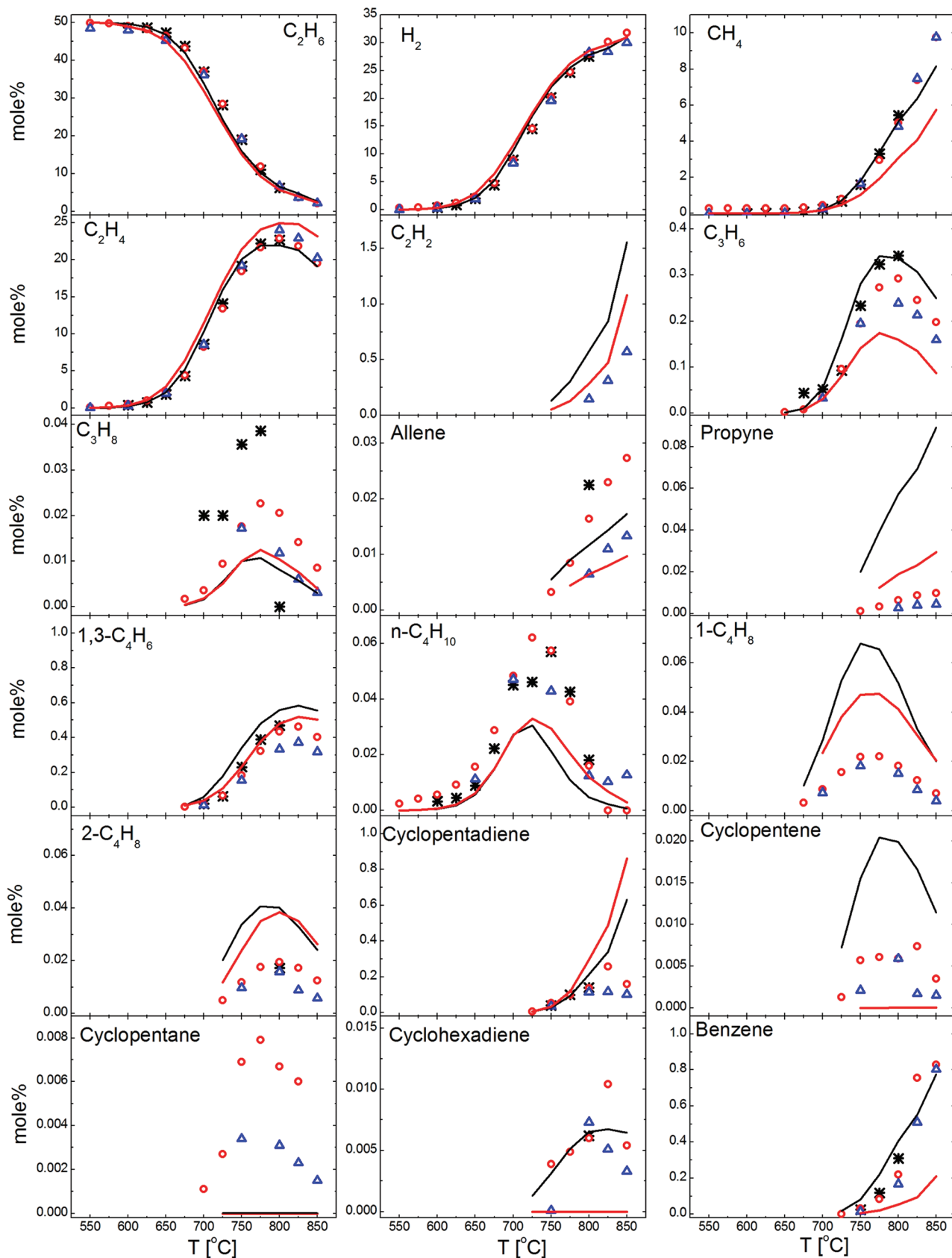


Figure 17. Comparison of measured mole fractions to those predicted with our updated mechanism (black) and to those obtained using the Jet Surf mechanism<sup>15</sup> (red).

to butadiene consumption. The reasons are similar to those discussed above for ethyl addition. Here, one expects even less of a contribution because the methyl concentration is significantly lower than ethyl. Thus, it would appear that the dominant reaction of butadiene to form higher molecular weight growth products is indeed the reaction with vinyl. This is due to the combination of a relatively large rate constant for the addition and, more importantly, the energetics of this system such that the adduct energy is much lower than the reactants energy for this special case of a high energy radical forming a resonantly stabilized adduct.

**4.7. Comparison to Literature Models.** Although there are many detailed models for hydrocarbon pyrolysis and oxidation, most of these were developed for conditions far removed from those employed in the current experiments, and these were validated against higher temperature experiments at much lower levels of conversion. We restrict our comparison to JetSurf 2.0,<sup>15</sup> a model resulting from an extensive collaboration among many institutions. Predictions with this mechanism are shown in Figure 17. The results for ethane and hydrogen are very similar to our updated model. JetSurf slightly overpredicts ethylene and underpredicts methane. Several of the C<sub>3</sub> species predictions are similar, with differences for propylene and propyne. The major difference is the substantial underprediction of cyclopentene, cyclohexadiene, and benzene production. This problem of an incomplete description of molecular weight growth is certainly not limited to JetSurf, and this comparison should not be taken as a criticism of that model, which was primarily developed to describe combustion kinetics. Rather, it may be used as an illustration of the importance of developing a proper description of molecular weight growth in a pyrolytic environment to provide an improved subset for combustion kinetic models.

**4.8. Comparison to Ethane Steam Cracking Data.** Sabbe et al.<sup>9</sup> measured product yields in a simulated pilot plant at pressures near 2 atm and compared these data to predictions using their mechanism. We have attempted to reproduce their conditions so as to compare the predictions of our model to their data as well as their predictions. One difference in this comparison is that we have nitrogen as the inert instead of the steam that was used in the experiments. The only effect of this change should be a reduction in the third body efficiencies for the pressure-dependent reactions. (We kept nitrogen as the inert because our pressure-dependent reaction analysis assumed this to be the collision partner.) Another difference is that we ignored any pressure drop along the reactor and assumed a constant pressure that was fixed at the reported outlet pressure. There was also some uncertainty introduced in reproducing their measured temperature profile. Given these differences, we decided that a more appropriate comparison consists of adjusting the reactant flow rate in the model until the amount of ethane reacted equaled that observed. We found that we needed to decrease the ethane flow rate from the reported 0.92 to 0.49 g/s, that is, increasing the residence time by a factor of ~1.9, to match the ethane conversion. Given the uncertainties, such an adjustment seems reasonable.

Our predictions are compared to the results of Sabbe et al. in Table 7. Overall, we find the agreement with our mechanism quite encouraging, suggesting that the Chebyshev representations of the pressure-dependent rate constants properly account for the impact of changing pressure. In many of the cases in which we see differences, the same trends are observed in comparison to our data, suggesting that it might be possible to improve the

**Table 7. Comparison of Predicted Mole Fractions to Gent Simulated Pilot Plant Data and Gent Simulations<sup>a</sup>**

species	observed (dry)	simulations (w/o inert)	
		Gent <sup>9</sup>	this work <sup>b</sup>
hydrogen	36.67	38.27	37.65
methane	3.66	2.11	3.06
acetylene	0.64	0.72	0.34
ethylene	33.50	34.35	33.78
ethane	24.29	23.55	23.60
propyne	0.019	0.014	0.045
allene	0.005	0.009	0.014
propylene	0.358	0.226	0.480
propane	0.038	0.017	0.021
1,3-butadiene	0.488	0.506	0.724
1-butene	0.040	0.023	0.103
n-butane	0.110	0.029	0.039
1,3-cyclopentadiene	0.034	0.031	0.040
benzene	0.145	0.145	0.106

<sup>a</sup> Gent conditions: ethane flow rate = 0.92 g/s, COT = 1101 K, COP = 1.91 E5 Pa. <sup>b</sup> Ethane flow rate decreased to 0.49 g/s to achieve ethane conversion comparable to that observed (cf. text).

agreement by adjusting appropriate rate constants within their range of uncertainties, but that is not the purpose of this effort. Rather, our intent is to demonstrate that one can capture much of the kinetics without any mechanistic adjustments, suggesting that overall structure of the mechanism is reasonable. However, one specific area that requires additional investigation is the over-prediction of butadiene; this might suggest the need for additional reactions of cyclopentadiene. Earlier, we saw that including the reaction of vinyl with cyclopentadiene had the effect of reducing the butadiene mole fraction, improving the fit to the data (cf. text, Figure 14).

**4.9. Reduced Mechanism.** The mechanism used to describe ethane pyrolysis was used earlier to describe more complex systems such as n-hexane and thus contains reactions that are not relevant for ethane. Moreover, the reasonably successful comparisons of this mechanism to ethane data only validate a relatively small subset of the overall mechanism. Thus, we have developed a reduced mechanism that only contains that subset of reactions required to describe ethane pyrolysis under the conditions employed in this work. This mechanism consists of 513 reactions and 49 species and is included in the Supporting Information. Over the temperature range from 550 to 850 °C, the predictions of this much smaller mechanism are in very good agreement with those of the complete updated mechanism. Slight discrepancies, on the order of 10% relative differences, were observed for some of the minor species. A larger version of the reduced mechanism, containing 1323 reactions and 125 species, predicts results virtually indistinguishable from the complete mechanism and is available upon request.

**4.10. Suggested Future Mechanism Improvements.** Examination of the comparisons in Figure 14 reveals several issues that require additional attention by researchers. One common deficiency is the underprediction of the higher alkanes (propane, butane, and cyclopentane). The rate analysis for propane and butane shows the dominant production channel to be radical recombination, with hydrogen abstraction by H atoms as the

primary loss channel. There is significant uncertainty regarding the pressure-dependent recombination rate constants, so these reactions should be explored in more detail. The situation is different for cyclopentane. Formation via radical recombination, such as ethyl + allyl, requires that the initially formed energized 1-pentene isomerizes to form cyclopentane. The barriers for such isomerization are substantial, and our preliminary analysis suggests this pathway will be too slow. Other pathways, such as initial formation of cyclopentyl, followed by hydrogen abstraction are currently included in the mechanism but cannot account for the observed production of cyclopentane. Perhaps this problem is related to the analysis of cyclopentane abstractions discussed earlier, where the CBS-QB3 results suggest that this rate constant is quite different from abstraction from linear alkanes. Another issue of some concern is the systematic overprediction of olefins. The updated radical addition pathways improved this situation in most cases, with the exception of cyclopentene, but additional attention is warranted.

## 5. CONCLUSIONS

The objective of this study was to analyze the gas-phase kinetics of ethane pyrolysis at high conversion with an emphasis on characterizing the kinetics of molecular weight growth. Our earlier kinetic model could quantitatively characterize ethane conversion and production of the major products hydrogen and ethylene. However, discrepancies in the description of C<sub>3</sub> and C<sub>4</sub> olefins lead us to initiate CBS-QB3 calculations of the C<sub>3</sub>H<sub>7</sub>, C<sub>4</sub>H<sub>7</sub>, C<sub>4</sub>H<sub>9</sub> potential energy surfaces and to extend the literature analysis for the C<sub>6</sub>H<sub>9</sub> PES. Inclusion of the results of these calculations significantly improved the model predictions for C<sub>3</sub> and C<sub>4</sub> olefins and the subsequent molecular weight growth to form benzene and cyclopentadiene. The reactions of 1,3-butadiene were identified as critical for molecular weight growth. A particularly important reaction is that of vinyl addition to butadiene. Another important observation is that several radical addition reactions are partially equilibrated. Not only does this mean that accurate thermodynamic parameters are essential for an accurate model, but that the description of a molecular weight growth pathway must include a final product that is sufficiently stable to shift the equilibrium toward the product despite the decrease in entropy that accompanies molecular weight growth. Interestingly, another important reaction, H addition to olefins, was found to inhibit molecular weight growth by leading to production of a lower olefin plus methyl radicals. This finding suggests that an important kinetic component is the ratio of hydrocarbon radicals (promoting growth) and H-atoms (inhibiting growth).

The overall reasonable agreement both to our data and to those of Sabbe et al. suggests that much of the kinetic behavior is captured by the current mechanism. One might certainly be able to improve some of the comparisons by adjusting rate constants within reasonable ranges, but that is not the point of this effort. Rather, we hoped to generate a mechanism based as close as possible to a fundamental understanding of the free radical reactions involved. We think that the overall level of agreement suggests that this is indeed the case and that the results of high-level calculations are sufficiently accurate to capture much of the essential kinetics. We are now in the process of extending this type of analysis to attempt to describe the pyrolysis kinetics, including molecular weight growth, of higher alkanes and alkenes.

## ■ ASSOCIATED CONTENT

**S Supporting Information.** Two forms of the reduced mechanism: one lists the rate constants in a modified Arrhenius form, suitable for use at 0.8 atm; the other lists the rate constants in a Chebyshev format that is applicable over a broad pressure range. Thermodynamic data for the species in the reduced mechanism. This material is available free of charge via the Internet at <http://pubs.acs.org>.

## ■ AUTHOR INFORMATION

### Corresponding Author

\*E-mail: amdean@mines.edu.

## ■ ACKNOWLEDGMENT

This work was supported by the Office of Naval Research under Grant No. N00014-05-1-0339, program officer Dr. Michele Anderson. Additional support was provided by the Abu Dhabi National Oil Co.

## ■ REFERENCES

- (1) Slagle, I. R.; Gutman, D.; Davies, J. W.; Pilling, M. J. *J. Phys. Chem.* **1988**, *92*, 2455–2462.
- (2) Wagner, A. F.; Wardlaw, D. M. *J. Phys. Chem.* **1988**, *92*, 2642–2471.
- (3) Wardlaw, D. M.; Marcus, R. A. *J. Phys. Chem.* **1986**, *90*, 5383–5393.
- (4) Robertson, S. H.; Wardlaw, D. M.; Hirst, D. M. *J. Chem. Phys.* **1993**, *99*, 7748–7761.
- (5) Oehlschlaeger, M. A.; Davidson, D. F.; Hanson, R. K. *Proc. Comb. Inst.* **2005**, *30*, 1119–1127.
- (6) Kiefer, J. H.; Santhanam, S.; Srinivasan, N. K.; Tranter, R. S.; Klippenstein, S. J.; Oehlschlaeger, M. A. *Proc. Comb. Inst.* **2005**, *30*, 1129–1135.
- (7) Hidaka, Y.; Sato, K.; Hoshikawa, H.; Nihimori, T.; Takahashi, R.; Tanaka, H. *Combust. Flame* **2000**, *120*, 245–264.
- (8) Tranter, R. S.; Raman, A.; Sivaramakrishnan, R.; Brezinsky, K. *Int. J. Chem. Kinet.* **2005**, *37*, 306–331.
- (9) Sabbe, M. K.; Van Geem, K. M.; Reyniers, M.-F.; Marin, G. B. *AIChE J.* **2011**, *57*, 482–496.
- (10) Glasier, G. F.; Pacey, P. D. *Carbon* **2001**, *39*, 15–23.
- (11) Matheu, D. M.; Grenda, J. M. *J. Phys. Chem. A* **2005**, *109*, 5332–5342.
- (12) Matheu, D. M.; Grenda, J. M. *J. Phys. Chem. A* **2005**, *109*, 5343–5351.
- (13) Wauters, S.; Marin, G. B. *Ind. Eng. Chem. Res.* **2002**, *41*, 2379–2391.
- (14) Sharma, S.; Harper, M. R.; Green, W. H. *Combust. Flame* **2010**, *157*, 1331–1345.
- (15) Egolfopoulos, F. N.; Wang, H.; Hanson, R. K.; Davidson, D. F.; Bowman, C. T.; Pitsch, H.; Law, C. K.; Cernansky, N. P.; Miller, D. L.; Tsang, W.; Lindstedt, R. P.; Violi, A. JetSurF version 2.0, September 19, 2010 (<http://melchior.usc.edu/JetSurF/JetSurF2.0>).
- (16) Villano, S. M.; Hoffmann, J.; Carstensen, H.; Dean, A. M. *J. Phys. Chem. A* **2010**, *114*, 6502–6514.
- (17) Randolph, K. L.; Dean, A. M. *Phys. Chem. Chem. Phys.* **2007**, *9*, 4245–4258.
- (18) Al-Shoabi, A. S. Ph.D. Thesis, Colorado School of Mines, 2008.
- (19) Carstensen, H.-H.; Dean, A. M. *J. Phys. Chem. A* **2009**, *113*, 367–380.
- (20) Venkatesh, P. K.; Chang, A. Y.; Dean, A. M.; Cohen, M. H.; Carr, R. W. *AIChE J.* **1997**, *43*, 1331–1340.
- (21) Chang, A. Y.; Bozzelli, J. W.; Dean, A. M. *Z. Phys. Chem.* **2000**, *214*, 1533–1568.
- (22) Carstensen, H.-H.; Dean, A. M. In *Comprehensive Chemical Kinetics*; Carr, R., Ed.; Elsevier: New York, 2007; Vol. 42, pp 105–187.

- (23) Ritter, E. R.; Bozzelli, J. W. *Int. J. Chem. Kinet.* **1991**, *23*, 767–778.
- (24) CHEMKIN-PRO; Reaction Design: San Diego, CA, 2008.
- (25) Baulch, D. L.; Bowman, C. T.; Cobos, C. J.; Cox, R. A.; Just, T.; Kerr, J. A.; Pilling, M. J.; Stocker, D.; Troe, J.; Tsang, W.; Walker, R. W.; Warnatz, J. *J. Phys. Chem. Ref. Data* **2005**, *34*, 757–1397.
- (26) Miller, J. A.; Klippenstein, S. J. *Phys. Chem. Chem. Phys.* **2004**, *6*, 1192–1202.
- (27) Baulch, D. L.; Cobos, C. J.; Cox, R. A.; Esser, C.; Frank, P.; Just, T.; Kerr, J. A.; Pilling, M. J.; Troe, J.; Walker, R. W.; Warnatz, J. *J. Phys. Chem. Ref. Data* **1994**, *23*, 847–1033.
- (28) Klippenstein, S. J.; Georgievskii, Y.; Harding, L. B. *Phys. Chem. Chem. Phys.* **2006**, *8*, 1133–1147.
- (29) Tsang, W.; Hampson, R. F. *J. Phys. Chem. Ref. Data* **1986**, *15*, 1087–1279.
- (30) Huynh, L. K.; Panasewicz, S.; Ratkiewicz, A.; Truong, T. N. *J. Phys. Chem. A* **2007**, *111*, 2156–2165.
- (31) Bhargava, A.; Westmoreland, P. R. *Combust. Flame* **1998**, *113*, 333–347.
- (32) Baulch, D. L.; Cobos, C. J.; Cox, R. A.; Frank, P.; Hayman, G.; Just, T.; Kerr, J. A.; Murrells, T.; Pilling, M. J.; Troe, J.; Walker, R. W.; Warnatz, J. *Combust. Flame* **1994**, *98*, 59–79.
- (33) Tsang, W. *J. Phys. Chem. Ref. Data* **1988**, *17*, 887–933.
- (34) Sutherland, J. W.; Su, M.-C.; Michael, J. V. *Int. J. Chem. Kinet.* **2001**, *33*, 669–684.
- (35) Baldwin, R. F.; Walker, R. W. *J. Chem. Soc., Faraday Trans. 1* **1979**, *75*, 140.
- (36) Curran, H. J. *Int. J. Chem. Kinet.* **2006**, *38*, 250–275.
- (37) Tsang, W. *J. Phys. Chem. Ref. Data* **1991**, *20*, 221–273.
- (38) Frisch, M. J.; Trucks, G. W.; Schlegel, H. B.; Scuseria, G. E.; Robb, M. A.; Cheeseman, J. R.; Montgomery, J. A., Jr.; Vreven, T.; Kudin, K. N.; Burant, J. C.; Millam, J. M.; Iyengar, S. S.; Tomasi, J.; Barone, V.; Mennucci, B.; Cossi, M.; Scalmani, G.; Rega, N.; Petersson, G. A.; Nakatsuji, H.; Hada, M.; Ehara, M.; Toyota, K.; Fukuda, R.; Hasegawa, J.; Ishida, M.; Nakajima, T.; Honda, Y.; Kitao, O.; Nakai, H.; Klene, M.; Li, X.; Knox, J. E.; Hratchian, H. P.; Cross, J. B.; Adamo, C.; Jaramillo, J.; Gomperts, R.; Stratmann, R. E.; Yazyev, O.; Austin, A. J.; Cammi, R.; Pomelli, C.; Ochterski, J. W.; Ayala, P. Y.; Morokuma, K.; Voth, G. A.; Salvador, P.; Dannenberg, J. J.; Zakrzewski, V. G.; Dapprich, S.; Daniels, A. D.; Strain, M. C.; Farkas, O.; Malick, D. K.; Rabuck, A. D.; Raghavachari, K.; Foresman, J. B.; Ortiz, J. V.; Cui, Q.; Baboul, A. G.; Clifford, S.; Cioslowski, J.; Stefanov, B. B.; Liu, G.; Liashenko, A.; Piskorz, P.; Komaromi, I.; Martin, R. L.; Fox, D. J.; Keith, T.; Al-Laham, M. A.; Peng, C. Y.; Nanayakkara, A.; Challacombe, M.; Gill, P. M. W.; Johnson, B.; Chen, W.; Wong, M. W.; Gonzalez, C.; Pople, J. A. *Gaussian 03*; Gaussian, Inc.: Pittsburgh, PA, 2003.
- (39) Zheng, X. B.; Blowers, P. *Ind. Eng. Chem. Res.* **2006**, *45*, 530–535.
- (40) Seakins, P. W.; Robertson, S. H.; Pilling, M. J.; Slagle, I. R.; Gmurczyk, G. W.; Bencsura, A.; Gutman, D.; Tsang, W. *J. Phys. Chem.* **1993**, *97*, 4450–4458.
- (41) Zheng, X. B.; Blowers, P. *Theor. Chem. Acc.* **2007**, *117*, 207–212.
- (42) Knyazev, V. D.; Slagle, I. R. *J. Phys. Chem.* **1996**, *100*, 5318–5328.
- (43) Tsang, W. *J. Phys. Chem. Ref. Data* **1990**, *19*, 1–68.
- (44) Gang, J.; Pilling, M. J.; Robertson, S. H. *J. Chem. Soc., Faraday Trans. 1* **1997**, *93*, 1481–1491.
- (45) Miller, J. L. *J. Phys. Chem. A* **2004**, *108*, 2268–2277.
- (46) Fahr, A.; Stein, S. E. *Proc. Combust. Inst.* **1989**, *22*, 1023–1029.
- (47) Shestov, A. A.; Popov, K. V.; Slagle, I. R.; Knyazev, V. D. *Chem. Phys. Lett.* **2005**, *408*, 339–343.
- (48) Ismail, H.; Goldsmith, C. F.; Abel, P. R.; Howe, P.; Fahr, A.; Halpern, J. B.; Jusinski, L. E.; Georgievskii, Y.; Taatjes, C. A.; Green, W. H. *J. Phys. Chem. A* **2007**, *111*, 6843–6851.
- (49) Cole, J. A.; Bittner, J. D.; Longwell, J. P.; Howard, J. B. *Combust. Flame* **1984**, *S6*, 51–70.
- (50) Cavallotti, C.; Rota, R.; Carra, S. *J. Phys. Chem. A* **2002**, *106*, 7769–7778.
- (51) Saeys, M.; Reyniers, M.; Marin, G. B.; Van Speybroeck, V.; Waroquier, M. *AIChE J.* **2004**, *50*, 426–444.
- (52) Sirjean, B.; Glaude, P. A.; Ruiz-Lopez, M. F.; Fournet, R. *J. Phys. Chem. A* **2006**, *110*, 12693–12704.
- (53) Tsang, W.; Mokrushin, V. *Proc. Combust. Inst.* **2000**, *28*, 1717–1723.
- (54) Lee, H. Y.; Kislov, V. V.; Lin, S. H.; Mebel, A. M.; Neumark, D. M. *Chem.-Eur. J.* **2003**, *9*, 726–740.
- (55) Hidaka, Y.; Higashihara, T.; Ninomiya, N.; Oshita, H.; Kawano, H. *J. Phys. Chem.* **1993**, *97*, 10977–10983.
- (56) Dayma, G.; Glaude, P. A.; Fournet, R.; Battin-Leclerc, F. *Int. J. Chem. Kinet.* **2003**, *35*, 273–285.
- (57) Goldsmith, C. F.; Ismail, H.; Green, W. H. *J. Phys. Chem. A* **2009**, *113*, 13357–13371.